Increased gut microbial mucin foraging promotes clearance of a parasitic worm

Short title: *Nematodes and gut microbial mucin foraging*

Mathis Wolter[a,b], Erica T. Grant[a,b], Amy Parrish[a,b], Alessandro De Sciscio[a], Seona Thompson[c,d], Marie Boudaud[a], Jean-Jacques Gerardy[e,f], Michel Mittelbronn[e,f,g,h,i,j], David J. Thornton[c,d], Andrew J. Macpherson[k,l,m], Richard K. Grencis[c,d] and Mahesh S. Desai[a,n,*]

[a]*Department of Infection and Immunity, Luxembourg Institute of Health, Esch-sur-Alzette, Luxembourg*

[b]*Faculty of Science, Technology and Medicine, University of Luxembourg, Esch-sur-Alzette, Luxembourg*

[c]*Lydia Becker Institute for Immunology and Inflammation. Faculty of Biology, Medicine and Health, University of Manchester, Manchester, United Kingdom*

[d]*Wellcome Centre for Cell Matrix Research, Faculty of Biology, Medicine and Health, University of Manchester, Manchester, United Kingdom*

[e]*National Center of Pathology, Laboratoire National de Santé, Dudelange, Luxembourg*

[f]*Luxembourg Center of Neuropathology, Dudelange, Luxembourg*

[g]*Luxembourg Centre for Systems Biomedecine, University of Luxembourg, Esch-sur-Alzette, Luxembourg*

[h]*Department of Cancer Research, Luxembourg Institute of Health, Luxembourg, Luxembourg*

[i]*Faculty of Science, Technology and Medecine, University of Luxembourg, Esch-sur-Alzette*

[j]*Department of Life Science and Medicine, University of Luxembourg, Esch-sur-Alzette, Luxembourg*

[k]*Department of Visceral Surgery and Medicine, Bern University Hospital, University of Bern, Bern, Switzerland*

[l]*Maurice Müller Laboratories, Department for Biomedical Research, University of Bern, Bern, Switzerland*

[m]*CMPG, Institute of Ecology and Evolution, University of Bern, Bern, Switzerland*

[n]*Odense Research Center for Anaphylaxis, Department of Dermatology and Allergy Center, Odense University Hospital, University of Southern Denmark, Odense, Denmark*

[*]Corresponding author: Mahesh S. Desai, mahesh.desai@lih.lu

Grant support

This work was supported by the following grants in the laboratory of M.S.D.: Luxembourg National Research Fund (FNR) CORE grants (C15/BM/10318186 and C18/BM/12585940) to M.S.D.; FNR PRIDE (17/11823097) and the Fondation du Pélican de Mie et Pierre Hippert-Faber, under the aegis of the Fondation de Luxembourg grants to E.T.G.; FNR AFR individual PhD fellowship to A.P. (11602973); and European Commission Horizon 2020 Marie Skłodowska-Curie Actions individual fellowship to M.B. (897408). MM thanks the Luxembourg National Research Fond (FNR) for the support (FNR PEARL P16/BM/11192868 grant). The Wellcome Trust supports work of R.K.G and S.T. (Z10661/Z/18/Z; 203128A/Z/16/Z) and D.J.T (203128A/Z/16/Z).

Correspondence

Mahesh S. Desai, PhD
Luxembourg Institute of Health
Department of Infection and Immunity
29, rue Henri Koch, L-4354 Esch-sur-Alzette
Luxembourg
Tel: +352 26970-389
Fax: +352 26970-390
Email: mahesh.desai@lih.lu

Disclosures

M.S.D. works as a consultant and an advisory board member at Theralution GmbH, Germany.

Author Contributions

M.S.D. supervised the study and obtained research funding; M.W., D.J.T., R.K.G. and M.S.D. conceived and designed the study; M.W., E.T.G., A.P., A.D.S., and S.T. performed the experiments; M.W., E.T.G., R.K.G., A.P. and M.B. analyzed the data; J.-J. G. and M.M. prepared slides for histology; A.J.M. supplied germ-free mice; M.W. and M.S.D. primarily

wrote the manuscript with input from E.T.G and A.P. All authors reviewed and approved the manuscript.

Data Transparency Statement

All data, study materials and analytical methods will be made available to other researchers upon request.

Abstract

BACKGROUND & AIMS

Host-secreted gastrointestinal mucus plays a key role in the expulsion of intestinal nematode parasites. A balance between mucin secretion by the host and the gut microbial mucin foraging is essential to maintain the intestinal homeostasis, yet little is known about how changes in the mucin–microbiome interactions affect worm infection. Here, we aimed to examine how increased mucin foraging activity by the microbiome changes the course of the parasitic infection by modulating the host immune responses.

METHODS

We employed a gnotobiotic mouse model containing a 14-member synthetic human gut microbiota that facilitates functional interpretations, including diet-driven manipulation of the microbiota toward mucin foraging. We infected the mice with a robust murine nematode, *Trichuris muris*, that closely resembles human infection with *Trichuris trichiura*. We investigated the temporal dynamics of worm infection including worm burden and the host immune responses, and connected these readouts to the microbial changes and metabolic activity toward mucin foraging.

RESULTS

The microbial mucin foraging was further increased during worm infection only in mice with pre-enhanced mucin degrading capacity. The elevated mucin foraging coincides with a shift in host immune responses from susceptible (chronic, Th1 type) to resistant (acute, Th2 type), which promotes worm clearance. The relative abundances of mucin-generalist bacteria drammatically increased during worm clearance, but not during worm retention.

CONCLUSIONS

These results point to a mechanism whereby skewing the metabolic activity of the microbiome toward mucin glycoproteins promotes resistance to worm infection. Our study documents a clinically-relevant, novel link in the microbiome–parasite–host immune axis, which is important prerequisite knowledge in treating parasitic infections.

Keywords

Mucin; gut microbiome; nematode; *Trichuris muris*

102 **Introduction**

103 Chronic infections by intestinal parasitic worms (helminths) are common in animals and
104 humans, especially in developing countries, where the infections are associated with high
105 morbidity[1]. Due to their ability to subvert the host immune response, helminths make an
106 invaluable model to study the host immunomodulatory mechanisms[2]. In this context, the
107 murine parasite *Trichuris muris*—a relevant biological model for the closely related human
108 parasite *Trichuris trichiura*—has been extensively investigated[3]. *T. muris* is an especially
109 attractive model as either a susceptible (chronic, Th1 type) or resistant (acute, Th2 type)
110 immune response is triggered, depending on the infectious dose[3,4]. Low-dose infections in
111 mice, which are more reflective of the naturally-occurring chronic infections[5], are generally
112 characterized by a Th1 response resulting in long-term worm infections and chronic colitis. On
113 the other hand, high-dose infections, which are employed as a laboratory model, are generally
114 characterized by an acute Th2 response leading to worm clearance and tissue repair[3].

115 Since they occupy the same host environment, it is no surprise that enteric parasites
116 such as helminths strongly interact with the gut microbiome[6,7]. Although these interactions may
117 lead to the suppression of either the gut microbiome or the helminth[6–8], in case of *T. muris*,
118 bacterial–helminth crosstalk is essential for worm hatching, as the parasite eggs fail to hatch
119 and establish in germ-free environments[9,10]. Once the worm has settled in the intestinal
120 epithelium, the bacterial–helminth dynamics appear mainly unidirectional, with helminths
121 altering the microbiome composition through various mechanisms, including through helminth
122 excretory-secretory products or host anti-microbial peptides, released in response to the
123 parasite[11–15]. Furthermore, the helminths alter the nutrients available to the microbiome,
124 indirectly influencing which bacteria proliferate[16]. The effect of the infection on host
125 immunology has an additional impact on the microbiome, as the worms or their metabolic
126 byproducts can alter toll-like receptor (TLR) expression profiles[17,18] or responsiveness of host
127 immune cells to TLR ligands[19] and interfere with local IgA-production[17]. While the
128 gastrointestinal (GI) mucins are essential for worm clearance[20–22] and the impacts of the
129 helminth infection on the microbiome during worm clearance are documented at the broader
130 level of microbial phylogeny[23–28], questions remain regarding how the mucus–microbiome
131 interactions affect worm infection and the underlying host immune responses.

132 Worm expulsion during an acute response is largely driven by goblet-cell secreted
133 gastrointestinal mucin that is tightly linked to the Th2-type immune response[22]. Along these
134 lines, mice lacking the *Muc2* gene, which encodes the major glycoprotein of the GI mucus,

135 show a delayed clearance of *T. muris*[29] and *Muc5ac* deficient mice completely fail to clear the
136 helminth[22]. In germ-free mice, the mucus layer expands upon exposure to gut bacteria, and the
137 colonic mucin secretion by goblet cells is regulated by the gut microbial activity[30,31]. The
138 balance between mucin secretion and its consumption by the gut microbes is critical for
139 intestinal homeostasis[32,33]. We have previously shown that a disrupted balance, for example,
140 excessive mucin foraging by a fiber-deprived microbiota leads to an increase in the gut
141 microbial mucin foraging activity[31,34].

142 Here, we hypothesized that excessive mucin foraging by the microbiota alters the
143 course of the parasite infection by modulating the immune response. To test this hypothesis,
144 we employed a tractable 14-member synthetic human microbiota (14SM) characterized for the
145 capability of individual members to degrade various glycans including mucin
146 oligosaccharides[31,35]. In a longitudinal experimental setup, using C57BL/6 ex-germ-free mice
147 with a homeostatic mucin-foraging 14SM, we induced a chronic *T. muris* infection.
148 Simultaneously, using fiber-deprived diet as a precursor, we skewed 14SM toward excessive
149 mucin foraging. We assessed the worm burden and immune outcome of infection. Moreover,
150 our 14SM model combined with a longitudinal infection setup enabled us to understand
151 specific microbial functional changes along the course of the infection in both homeostatic
152 14SM and 14SM skewed toward mucin foraging. Our findings suggest a mechanism through
153 which the increased gut microbial mucin foraging promotes worm clearance by enhancing a
154 Th2 immune response, which sheds a new light on the microbiome–parasite–host immune
155 interactions.
156

157 **Methods**

158 ***Ethical statement***

159 All animal experiments were performed according to the "Règlement Grand-Ducal du 11
160 janvier 2013 relatif à la protection des animaux utilisés à des fins scientifiques" based on
161 Directive 2010/63/EU on the protection of animals used for scientific purposes, and approved
162 by the Animal Experimentation Ethics Committee of the University of Luxembourg and by the
163 Luxembourgish Ministry of Agriculture, Viticulture, and Rural Development (national
164 authorization no. LUPA2020/02). The mice were housed in accordance with the
165 recommendations stated by the Federation of European Laboratory Animal Science
166 Associations (FELASA).
167

168 ***Experimental design and dietary treatment***

169 18–23 weeks old C57BL/6 male mice (n=4–5 per group) were housed in ISOcages with up to
170 five animals per cage. Sterile food and water were provided *ad libitum* and light cycles
171 consisted of 12 hours. Before the administration of 14SM, the germ-free status of the mice was
172 confirmed using aerobic and anaerobic culturing of stools samples. Mice were intragastrically
173 gavaged with 0.2 ml of the 14SM gavage mix as described previously[35]. Before and for 6 days
174 following the gavage, mice were maintained on a standard mouse chow, which we refer to as
175 Fiber-rich (FR) diet. Afterwards, half of the mice (n=24) were assigned to a Fiber-free (FF)
176 diet and the rest remained on the FR diet (n=23). Twenty days after the diet switch, the mice
177 were infected by oral gavage with a high dose of approximately 450 eggs of *T. muris* strain E.
178 Mice were observed for up to 30 days post-infection (DPI). On 13, 15, 20, 25 and 30 DPI, four
179 to five mice per group were euthanized by cervical dislocation to determine worm counts and
180 other final readouts. A small piece (~0.5 cm) of the cecum was fixed in methacarn fixative in
181 order to determine goblet cell numbers. The remaining part of the cecum and 2 cm of the
182 attached colon were frozen at –80 °C to determine *T. muris* worm burden. The remaining
183 colonic tissue and mesenteric lymph nodes were stored in RNAprotect Tissue Reagent (Qiagen,
184 Hilden, Germany; catalog no. 76106, according to the manufacturer's protocol). Serum of the
185 euthanized mice was collected and stored at –80 °C.

186

187 ***Animal diets***

188 The Fiber-rich diet was a standard autoclaved rodent chow (LabDiet, St. Louis, MO, USA;
189 catalog no. 5013), while the Fiber-free diet was a custom diet manufactured and irradiated by
190 SAFE Diets (Augy, France). The FF diet was manufactured as the previously described
191 TD.140343 diet[31], which is a modified version of the Harlan.TD08810 diet from Envigo
192 (Indianapolis, IN, USA).

193

194 ***14SM cultivation and quantification***

195 All bacterial strains of the 14SM were cultured as previously described[35]. The colonization of
196 the 14SM was confirmed using strain-specific qPCR primers and relative abundances of the
197 individual bacteria were determined using the same qPCR protocol as described previously[35].
198 Samples from different dates were run on the same plates in order to avoid plate-specific
199 confounders.

200

201 ***Parasitological techniques***

202 *T. muris* maintenance and infection was performed as previously described[36]. Mice were orally
203 infected with ~450 eggs and worm burdens were assessed by counting the number of worms
204 present in the cecum and 2 cm of the attached colon as described previously[36]. Worm burdens
205 on 13 and 15 DPI were excluded from the analysis as determining the burden during the early
206 larval stages, where low worm numbers establish, is technically challenging and is unreliable.
207 The researcher, S.T., who counted the worms, was blinded for both the individual time points
208 and dietary groups.

209

210 ***Goblet cell counting***

211 Goblet cell counting was performed on a small piece (~0.5 cm) of methacarn-fixed and Alcian
212 blue-stained cecal tissue. To preserve the mucus within the intestinal samples, a modified direct
213 pretreatment in 99% ethanol and toluene was performed, omitting the usual previous ascending
214 ethanol steps before embedding the samples in paraffin. All samples were cut using a
215 microtome at 3 µm thickness before performing automated HE (Tissue-Tek Prisma Plus and
216 Film, Sakura, Alphen aan den Rijn, Netherlands) and Alcian blue (Artisan Link Pro Special
217 Staining System, Dako, Glostrup, Denmark) staining according to the manufacturers'
218 instructions. The numbers of goblet cells per crypt were counted and averaged for each
219 individual mouse before the mean per experimental group was determined. The researcher,
220 S.T., who counted the goblet cells, was blinded for both the individual time points and dietary
221 groups.

222

223 ***ELISA***

224 Lipocalin-2 ELISA was performed on stool samples using the lipocalin-2/NGAL DuoSet
225 ELISA R&D system (Bio-Techne, Minneapolis, MN, USA; catalog no. DY1857) according to
226 the manufacturer's instructions and samples were prepared as previously described[31]. MCPT1
227 concentration of serum samples was determined using the MCPT-1 (mMCP-1) Mouse
228 Uncoated ELISA Kit from Invitrogen (Waltham, MA, United States, catalog. no. 88-7503-88)
229 according to manufacturer's instructions. Serum ELISA for total IgG1 and IgE were performed
230 by coating plates using 0.5 µg/µl rat α mouse IgE purified UNLB (Imtec Diagnostics, 1130-
231 01) or rat α-mouse IgG1 purified UNLB (Imtec Diagnostics, Ardmore, OK, United States;
232 catalog no. 1144-01) capture antibody diluted in 0.05 M carbonate/bicarbonate buffer (pH 9.6).
233 Washing steps were performed using 1% Tween, 154 mM NaCl, 10 mM Trizma Base.
234 Blocking of the plates was performed using 1% w/v of BSA in a TBS buffer (15 mM Trizma-

235 acetate, 136 mM NaCl & 2 mM KCl). Mouse IgG1 Isotype Control UNLB (Imtec Diagnostics,
236 Ardmore, OK, United States; catalog no 0102-01) or Mouse IgE Isotype Control (UNLB),
237 Southern Biotech (Imtec Diagnostics, Ardmore, OK, United States; catalog no 0114-01) served
238 as controls. Serum samples were two-fold diluted using the aforementioned TBS buffer with
239 0.1% w/v Tween-20 and 1% BSA. The secondary antibody was Goat anti-mouse IgG1-AP,
240 Southern Biotech (Imtec diagnostics, Ardmore, OK, United States; catalog no 1071-04) or Goat
241 anti-mouse IgE-AP, Southern Biotech (Imtec diagnostics, Ardmore, OK, United States; catalog
242 no 1110-04), respectively. The substrate solution consisting of 0.5 mg/ml phosphate substrate
243 (Sigma-Aldrich, St. Louis, MO, United States; catalog no. S0642-200 TAB) in 1 mM AMP
244 and 0.1 mM $MgCl_2 \cdot 6H_2O$ and plates were read at 405 nm using a SpectraMax ABS PLUS
245 spectrophotometer (Molecular Devices, San Jose, CA, United States). A detailed protocol can
246 be found in the supplementary methods section. Parasite specific IgG1 and IgG2c ELISA was
247 performed as previously described[37].
248
249 ***LEGENDplex bead-based immunoassay***
250 The LEGENDplex assay (BioLegend, San Diego, CA, USA) was performed on serum samples
251 according to manufacturers' instruction.
252
253 ***Detection of bacterial glycan-degrading enzyme activities***
254 The enzymatic activities of α-fucosidase, β-*N*-acetyl-glucosaminidase, and β-glucosidase in
255 fecal samples were determined using *p*-nitrophenyl glycoside-based enzyme assays as
256 described previously[38].
257
258 ***RNA extraction from mesenteric lymph nodes and colonic tissue and RT-qPCR***
259 A detailed protocol can be found in the supplemental methods section.
260
261 ***RNA-Seq***
262 RNA extracted from samples at 30 DPI were utilized for performing RNA-Seq. Illumina
263 Stranded Total RNA Prep with Ribo-Zero Plus was used to prepare the RNA sequencing library
264 according to the reference guide's instructions. Sequencing was performed using NovaSeq
265 6000 SP Reagent Kit v1.5 (Illumina, San Diego, CA, USA) on an Illumina NovaSeq 6000
266 system.
267
268 ***RNA-Seq analysis***

Following adapter removal with Cutadapt[39], reads were mapped and gene counts were generated with STAR 2.7.9a[40]. Transcripts not appearing at least once on average across all samples were removed from subsequent analysis. Samples were normalized using the median of ratios method[41] supported by DESeq2[42] and one outlier was removed based on PC score using the prcomp function of the base R stats 4.0.2 package. Differential expression analysis was performed using DESeq2 1.30.1 with default parameters and *p*-value adjustment using the Benjamini-Hochberg method. Significant genes were identified based on adjusted *p*-value < 0.05. The expressed log-ratios for significant genes were imported into Ingenuity Pathway Analysis (Qiagen, Hilden, Germany) and analyzed considering all available reference datasets for mice. Pathway analysis was also performed using the enrichGO function of clusterProfiler 3.18.1[43] in R to identify upregulated pathways using Gene Ontology (GO) terms for biological processes. REVIGO[44] was employed to reduce redundancy in GO terms before visualisation.

Statistical analyses

Statistical analysis was performed using Prism 9.2.0. (GraphPad Software, Inc., San Diego, CA, USA), Statistical significances are represented by asterisks as follows: *, $p < 0.05$; **, $p < 0.01$; ***, $p < 0.001$; and ****, $p < 0.0001$. Unless otherwise specified in the figure legend, for normally distributed values, unpaired two-tailed t tests were used, while for non-normally distributed values, a Mann–Whitney test was used. For multiple comparisons, a two-way analysis of variance (ANOVA) with a Šidák post hoc test was performed in Prism. The specific test used for each experiment is detailed in the figure legends.

290 **Results**

291 ***Increased mucin-degrading bacteria coincides with altered worm infection dynamics***

292 We colonized germ-free, C57BL/6 mice with a 14-member synthetic human microbiota
293 (14SM). Successful colonization of each bacterial strain was checked by qPCR primers specific
294 to each of the 14 bacterial strains as described previously[35]. Mice were maintained for six days
295 on the Fiber-rich (FR) diet, which is a standard mouse chow, before half of the mice (n=24)
296 were switched to a Fiber-free (FF) diet **(Fig. 1A)**. Twenty days after the diet switch, mice in
297 both dietary groups were gavaged with a high dose of *T. muris* consisting of approximately 450
298 eggs from the same egg suspension **(Fig. 1A)**. Mice were monitored for up to 30 days post-
299 infection (DPI) and, on 13, 15, 20, 25 and 30 DPI, 4–5 mice per group were sacrificed and
300 cecum, colon and mesenteric lymph nodes (MLNs) were frozen in order to collect various
301 experimental readouts **(Fig. 1A)**. In line with our published work[31,45], the FF diet allowed for
302 proliferation of two dominant mucin-degrading bacteria *Akkermansia muciniphila* and
303 *Bacteroides caccae* and reduction of two prominent fiber-degrading bacteria *Eubacterium*
304 *rectale* and *Bacteroides ovatus* **(Fig. 1B)**. Throughout the experiment, none of the mice
305 exhibited any obvious physiological abnormalities. While FF-fed mice were overall heavier
306 compared to the FR-fed mice, the weights of both groups remained largely stable over time
307 **(Fig. 1C)**.

308 Frozen cecal tissues, including the ascending colon containing their luminal contents,
309 were defrosted and the worms were counted in a blinded fashion. Following the establishment
310 of low level infections, during the early larval stages, the *T. muris* larvae are too small to allow
311 reliable enumeration which is why the worm burdens were only assessed starting day 20 post
312 infection. Infection of *T. muris* with a high egg number (~450) in conventional or specific-
313 pathogen-free (SPF) mice, results in an acute infection, and only lower number of eggs (<40)
314 result in a chronic infection[3]. In our synthetic human gut microbiota under standard dietary
315 conditions (that is fed the FR diet), infection with a high number of eggs caused a low level
316 infection resulting in a chronic infection. The reasons for this could be rooted in an initially
317 skewed immune response in our gnotobiotic model or in the fact that our study uses a synthetic
318 human gut microbiota, as opposed to the complete, native murine microbiota that may be more
319 suitable for egg hatching of the naturally occurring murine whipworm or improving the ability
320 of the larvae to establish in the gut. Considering that this a new model, it is particularly an
321 important point because previous studies have shown that the gut bacteria are essential for
322 effective egg hatching, as the eggs do not hatch in the absence of gut bacteria *in vitro* or in

323 germ-free mice[9,10]. Our results showed that, although the worm burdens were statistically
324 insignificant between FR and FF groups on 20 and 25 DPI, subsequent infection dynamics
325 statistically differed between both groups, with FF-fed mice clearing the pathogen by 30 DPI
326 and FR-fed mice remaining chronically infected **(Fig. 1D)**.

327 In order to investigate whether the two distinct diets and/or the skewed gut microbiome
328 composition toward mucin polymer degradation caused an altered baseline inflammation prior
329 to infection with *T. muris*, we determined fecal lipocalin-2 (LCN-2) levels, which serves as a
330 marker for low-grade inflammation[46]. There were no significant differences between FR and
331 FF groups at day 0 **(Fig. 1E)**, which is in line with our previous results in C57BL/6 mice[45].
332 However, after the infection, the levels of LCN-2 were significantly higher in the FR group
333 **(Fig. 1E)**. Since chronic *T. muris* infections are characterized by a Th1 response leading to
334 colitis, the elevated LCN-2 in the FR group compared to the FF group is indicative of an early
335 induction of a Th1 response in the FR group, because LCN-2 has been shown to be induced by
336 the Th1 cytokines IFNγ and TNF-α[47]. Altogether, these results are supportive of the notion that
337 the worm retention in FR-fed 14SM group is driven by a Th1 immune response and similarly
338 the worm clearance in FF-fed 14SM group might be driven by a Th2 response.
339

340 ***Global transcriptomic analyses support chronic and acute outcomes of worm infection***

341 In order to better understand the change in host immunological responses that drive differential
342 *T. muris* infection dynamics, we analyzed the host colonic gene expression at 30 DPI **(Fig. 2,**
343 **Fig. S1 and Table S1)**. We found numerous significant differences in the host transcriptome
344 of FR- and FF-fed mice, as evident in the volcano plot showing the differentially expressed
345 genes, with 147 and 184 genes upregulated in the FR- and FF-fed groups, respectively **(Fig**
346 **2A)**. Ingenuity Pathway Analysis (IPA) revealed that both the interferon signaling and Th1
347 pathways were upregulated in the FR-fed mice that had a homeostatic 14SM before infection
348 **(Fig. 2B)**. These two pathways are characteristic of chronic *T. muris* infections[3], which was
349 consistent with the failure to successfully clear the parasite among FR-fed mice **(Fig. 2B)**. In
350 accordance with upregulation of the interferon signaling and Th1 pathways, related disease
351 pathways—that is, diseases often associated with an increased Th1 response such as
352 osteoarthritis, systemic lupus erythematosus and even neuroinflammation—were also
353 upregulated as their gene expression profiles overlap with those of a Th1 response **(Fig. 2B)**.

354 A closer look at the Ingenuity-generated summary of the transcriptomic data using IPA,
355 showed that indeed most of the genes upregulated under FR conditions during the chronic *T.*

356 *muris* infection are strongly linked to interferon signaling, which results in a Th1 response **(Fig.**
357 **2C)**. This Th1 response is potentially linked to the observed increase in antimicrobial responses
358 that results in the activation of cytotoxic T cells, lymphopoiesis, increased apoptosis of
359 macrophages and a reduced replication of viruses **(Fig. 2C)**. In contrast to this, the host
360 transcriptomic response on the FF diet was not clearly characterized by an increased Th2-type
361 response typical for an acute *T. muris* infection **(Fig. 2B)**. However, the moderate type 2
362 response might be a result of the chosen sample time point as the infection is mostly cleared
363 by 30 DPI **(Fig. 1D)**. In line with this, the increased MSP-RON signaling in macrophage
364 pathway hints at an increased Th2 response under FF conditions **(Fig. 2B),** as an activation of
365 the MSP-RON pathway causes M2 macrophage polarization[48], which is associated with a Th2-
366 type immune response against *T. muris*[49,50]. Furthermore, the upregulation of the white adipose
367 tissue browning pathway is also in line with this observation, as M2 macrophage differentiation
368 has been linked to adaptive thermogenesis[51]. The observed results are consistent with a major
369 shift toward the Th1 pathway and a chronic infection in the FR-fed group, whereas the acute
370 response observed in the FF-fed group seems most likely to be based on the Th2 immunity or
371 a failure to generate the Th1 immunity.
372
373 ***Maintenance or moderate increase of Th2 immunity permits worm expulsion***
374 In order to further support conclusions from our RNA-Seq data **(Fig. 2)**, we used RT-qPCR to
375 investigate transcription of cytokines IFNγ, IL-13 and IL-4 in RNA extracted from MLNs and
376 colon at different time points **(Fig. 3A)**. These three cytokines are indicative of whether *T.*
377 *muris* infection leads to a Th1- (IFNγ) or a Th2-type response (IL-4 and IL-13)[50,52]. In
378 accordance with the global transcriptome analysis **(Fig. 2)**, chronic infection in the FR-fed
379 group was dominated by a Th1-type response, as exhibited by over 6-fold upregulation of IFNγ
380 in the colon by 30 DPI **(Fig. 3A)**. Cytokine expression in the MLNs was even more
381 pronounced, with IFNγ having an over 30-fold increase in the FR group at day 20 and dropping
382 to a 6-fold increase at 30 DPI. IL-13 was only significantly upregulated in the MLNs of FF-fed
383 mice at 20 DPI and IL-4 showed a significant increase in the MLNs of the FR group at D15
384 before being upregulated under FF conditions for the subsequent days **(Fig. 3A)**. We performed
385 similar analysis of the cytokine transcripts of TNF-α, IL-5, IL-22 and IL-17a at 13 and 30 DPI,
386 but only TNF-α showed significant changes, with upregulation in the colon of the FR group
387 both at 13 and 30 DPI **(Fig. S2A)**. No diet-independent shifts in cytokine production were
388 found by analyzing the absolute cytokine data **(Fig. S3)**.

389 To lend support to our transcript data, we used the LEGENDplex bead-based
390 immunoassay to determine the cytokine protein concentration in the serum samples of mice at
391 30 DPI. Only one of the detected Th1 cytokines, TNF-α, was significantly upregulated under
392 FR conditions **(Fig. 3B)** and another Th1 cytokine, IFNγ, showed an upward trend with
393 p=0.0587. Some of the detected cytokines showed a trend toward increased production under
394 the FR conditions, hinting at a generally more active immune system during the chronic
395 infection **(Fig. 3B and Fig. S2B)**. The expression of transcription factors GATA3 and Tbet
396 **(Fig. S2C)** further supports these trends by showing significantly increased levels of Tbet
397 expression in the colon of the FR group at 30 DPI and a significant increase in GATA3 in the
398 MLN of the FF group at 20 DPI **(Fig. S2C)**.
399 Assessment of serum concentrations of total IgE and IgG1, both of which are reflective
400 of the protective responses against helminths, such as *T. muris*, resulted in no significant
401 changes, albeit a slightly increased trend was observed for both antibodies at 30 DPI but not at
402 25 DPI **(Fig. 3C)**. We then assessed parasite specific IgG1and IgG2, characteristic of Th2 and
403 Th1 responses, respectively[53]. Chronic *T. muris* infections are usually characterized by
404 significantly elevated serum levels of parasite-specific IgG2a/c and a low increase in parasite
405 specific IgG1[53]. In contrast, protection against *T. muris* is characterized by high parasite
406 specific IgG1 levels, but a lack of IgG2a/c[53]. Importantly, although there was no significant
407 increase in total IgG1, *T. muris*-specific IgG1 and IgG2a/c showed clear significant differences
408 at 30 DPI, but not at 25 DPI **(Fig. 3D)**. In accordance with the observed worm burdens **(Fig.
409 1D)**, we saw an increase in specific IgG1 in mice fed the FF diet, while we see an increase in
410 specific IgG2a/c in mice fed the FR diet **(Fig. 3D)**. Despite a similar upward trend for both
411 parasite-specific antibodies at 25 DPI in the two respective dietary groups, the differences were
412 not significant **(Fig. 3D)**. Furthermore, we quantified MCPT1—a proxy for mast cell
413 degranulation[54]—in sera at all time points (13, 15, 20, 25 and 30 DPI) and observed
414 significantly increased MCPT1 concentration at 30 DPI in the FF-fed group that cleared the
415 parasite **(Fig. 3E)**. These data are in line with an increased tendency of total IgE in the FF-fed
416 group at 30 DPI. Moreover, these data support the known association of mucosal mast cells
417 and protection against helminths[55,56] supporting the elevation of the type 2 immunity.

418 Overall, our transcript **(Fig. 2 and Fig. 3A)** and protein expression data **(Fig. 3B)**
419 support that, mostly during the later stages of infection, the worm infection in mice containing
420 a homeostatic 14SM induce a Th1-type immune response that is driven by an overall increase
421 in IFNγ. On the other hand, absence of a similar increase in IFNγ, after the worm infection, in

422 mice with increased microbial mucin foraging, induces a Th2-type immune response, resulting
423 in the successful clearance of *T. muris*. This heightened Th2 response seems to peak earlier
424 compared to the Th1 response of the FR group and likely levels off by 30 DPI; thus, the 30
425 DPI transcriptomics data **(Fig. 2)** might not have fully captured the Th2 response. Since the gut
426 microbiome is intimately connected to changes in the diet and the host immune responses, and
427 since specific changes in the microbial taxa could contribute to the observed immune
428 responses, we ventured to determine which bacteria change in their abundance during the
429 course of the worm infection.
430
431 ***Mucin generalists increase during worm clearance, but not during worm retention***
432 Although previous studies have reported noticeable changes in the gut microbial taxa in mice
433 with conventional gut microbiota after worm infection, these changes are described at broader
434 level of microbial taxonomy[23–28]. It also remains to be studied which precise microbial species
435 respond most to worm infection particularly during a longitudinal course of the worm infection
436 both during chronic and acute phases of infection. Better understanding such changes would
437 aid in further exploration of the microbiota–worm–host immune system interactions. In this
438 regard, our tractable, fully-characterized 14SM model[31] is well-suited to support functional
439 interpretations of how the underlying microbial metabolism changes as the worms start to
440 moult and are either expelled (acute infection) or remain persistent (chronic infection). Thus,
441 we next investigated the fecal gut microbial compositions using specific qPCR primers for all
442 five time points post infection (13, 15, 20, 25 and 30 DPI) in both dietary groups **(Fig. 4).** To
443 facilitate comparison, we combined these data with the microbial compositions prior to worm
444 infection in Fig. 1B (shown in Fig. 4 as day 0).

445 Throughout the experiment, the gut microbiome composition in the mice that had been
446 FR-fed for 20 days prior to infection remained distinct from the composition of the FF-fed mice
447 as seen in the principal coordinates analysis (PCoA) plots **(Fig. 4A)**. While the 14SM
448 composition has been shown to be stable over time[31], here we show that infection with *T. muris*
449 led to substantial changes in the gut microbiome composition within each dietary group **(Fig.**
450 **4A)**. These changes seemed to be more dynamic under FF conditions than under FR conditions,
451 which is likely explained by the nature of the chronic infection under FR conditions and an
452 acute infection in the FF conditions, but might also be reflective of the worm burden of
453 individual mice **(Fig. 4A)**. Looking at the microbiome composition over the course of the
454 infection, while diet impacts the initial colonization of the gut microbiome, the infection with

455 *T. muris* led to the bloom of some bacterial species and a decline of others **(Fig. 4B)**.
456 Interestingly, some of these changes seem to revert to initial levels upon clearance of *T. muris*
457 in the mice fed the FF diet **(Fig. 4A and 4B)**.

458 Most of the individual bacteria changed in relative abundance either in response to the
459 early larval stages (L2 (~day 8/9)–L3 (~day 17)) of *T. muris* or in response to the later larval
460 stages (L3–L4 (~day 23)) **(Fig. 4C)**. These infection-induced abundance changes seem to be
461 reversible for most bacteria **(Fig. 4C)**. *Marvinbryantia formatexigens* appears to be an
462 exception as it does not significantly change in relative abundance due to either diet or infection
463 **(Fig. 4C)**. Considering that we observed that nearly all bacteria change in abundance during
464 the early larval stages of *T. muris*, it is likely that the growing worms competitively take over
465 certain nutrients. While the overall bacterial abundances are modulated by the diet
466 composition, some bacteria such as *Collinsella aerofaciens* or *Escherichia coli* seemed
467 unaffected by diet. It has been reported that tissue damage induced by *T. muris* might induce
468 the hypoxia response gene HIF-1α[57]. The resulting increased oxygen availability might explain
469 the diet-independent bloom of the facultative anaerobic *E. coli*, just after the infection **(Fig.**
470 **4C)**. Furthermore, other highly oxygen sensitive bacteria such as *Roseburia intestinalis* and
471 *Faecalibacterium prausnitzii* dropped in abundance around the same time, while the more
472 oxygen-resistant *Bacteroides* spp. remained largely unaffected **(Fig. 4C)**[58].

473 Among the bacteria with mucin-degrading capacities, we observed that the abundance
474 of *B. caccae* and *Bacteroides thetaiotaomicron* increased in the FF-fed group during the course
475 of the infection, but not in the FR-fed group **(Fig. 4C)**. The normalized average fold-change of
476 the abundance of these two mucin-generalist bacteria (*B. caccae* and *B. thetaiotaomicron*)[31]
477 significantly increased by 15 DPI and kept increasing until doubling their abundance at 20 DPI
478 in the FF-fed group but not in the FR fed group **(Fig 4D)**. In contrast, the abundance of mucin
479 specialist, *A. muciniphila* slightly decreased in the FF-fed group **(Fig 4C)**. Since being a mucin-
480 generalist and being capable of removing sulfate linkages on mucins[59] as well as secreting M-
481 60 like proteases that degrade the mucin protein backbone[31,32], *B. caccae* and *B.*
482 *thetaiotaomicron* are more aggressive mucin foragers than *A. muciniphila*, especially in the
483 absence of dietary fibers. These data suggest an overall increased mucin-foraging activity in
484 the FF-fed group as the worms start to grow and moult. This is further supported by the halted
485 expansion of the mucin-specialist *Barnesiella intestinihominis* at 15 DPI in the FF group **(Fig**
486 **4C)**. A sharp significant increase in the abundance of a sulfate-reducing bacterium
487 *Desulfovibrio piger* on 20 DPI in the FF-fed group, but not in the FR-fed group, further supports

488 the increase in mucin-foraging, as this bacterium increasingly utilizes the released sulfate from
489 microbial mucin foraging as an electron acceptor[60].

490 Intriguingly, even in the absence of fiber, a classical fiber-degrader *E. rectale* bloomed
491 in the FF-fed group around 25 DPI, after being almost non-existent before this and finally
492 became almost non-existent again on 30 DPI **(Fig. 4C)**. This coincides with the bloom of the
493 mucin generalists **(Fig. 4C)**. A similar trend was observed for *E. rectale* in the FR-fed group
494 **(Fig. 4C)**, with the abundance of *E. rectale* doubling in the FR-fed group as compared to its
495 abundance at 0 DPI. We have previously shown that *E. rectale* is adept at growing on two
496 mucosal monosaccharides, galactose and *N*-acetylglucosamine, but it fails to grow on mucin
497 oligosaccharides[31]. A potential explanation for the dramatic increase in *E. rectale* is that,
498 despite an absence of dietary fibers in the FF-fed group, simple mucin sugars that can be readily
499 metabolized, such as galactose and *N*-acetylglucosamine, become readily available through the
500 elevated mucin degradation in the FF-fed group at around 20 DPI by the two mucin generalists
501 *B. caccae* and *B. thetaiotaomicron*. Considering that the expansion of *E. rectale* occurs under
502 both diets, another supportive explanation is that the *T. muris*-secreted serine proteases, which
503 can depolymerize mucin[21], may make these structurally complex glycoproteins accessible to
504 bacteria that are otherwise unable to utilize them, such as *E. rectale*. The loss of exclusivity of
505 this niche offers a potential explanation for the halted expansion of the mucin specialists, *A.*
506 *muciniphila* and *B. intestinihominis* **(Fig. 4D)**. Collectively, these results strongly connect
507 increased mucin-degrading bacterial activity to worm clearance in the FF-fed group. As mucin
508 plays a key role in the clearance of *T. muris* infection, we next rationalized that enhanced
509 mucolytic activity during infection leads to increased mucus turnover, meaning an increased
510 cycle of mucin degradation and secretion, which could facilitate clearance of *T. muris* in the
511 FF-fed mice.

512

513 ***Enhanced mucin–microbiome interactions promote worm clearance***

514 Since we found that the worm clearance is strongly correlated to increased abundance of
515 mucin-degrading generalist bacteria, we next set out to study how this altered microbial
516 composition has a functional impact on the mucin-degrading activity. To assess this, we
517 measured the enzyme activity of the key mucin-degrading bacterial enzymes β-*N*-
518 acetylglucosaminidase (NAG) and α-fucosidase (FUC) before and at days 20 and 25 post-
519 infection **(Fig. 5A)**. As a contrast to these key mucin-degrading enzymes, we similarly
520 determined the activity of β-glucosidase (GLU), a microbial enzyme specific for plant

521 polysaccharides **(Fig. 5A)**. At day 0, NAG activity was higher under FF conditions; however,
522 after the infection, the activity of this enzyme significantly rose by 25 DPI in mice resistant to
523 persistent worm infection, but not in the mice where worm infection became chronic. A similar
524 pattern was observed for FUC activity. In contrast, GLUC activity showed a significant
525 increase in the resistant mice only at 20 DPI **(Fig. 5A)**. Comparing NAG and FUC activity
526 **(Fig. 5A)** to the abundance of mucin-degrading bacteria **(Fig. 4C and D)**, we observed a delay
527 between the increased abundance of mucin-generalist bacteria under FF conditions at 20 DPI
528 and the increased activity of mucin-degrading enzymes at 25 DPI, possibly due to a slight delay
529 in extracellular secretion of the enzymes into the feces. A potential explanation is the tight
530 regulation of mucin-degrading enzymes, as observed for *B. thetaiotaomicron*[61]. The
531 depolymerized mucin released by the serine proteases of *T. muris* might initially suppress the
532 expression of the NAG and FUC until fiber-degrading bacteria such as *E. rectale* expand
533 sufficiently to fully scavenge those glycans[61]. Looking at the strong increase in the relative
534 abundance of some fiber-degrading bacteria, such as *E. rectale,* around 20 DPI, it is also
535 possible that the absolute abundance of the mucin-degrading bacteria under FF conditions
536 keeps increasing past 20 DPI, but that this continuous expansion is not observable in the
537 relative abundance due to an even stronger expansion of other bacteria (**Fig 4C and D)**. In this
538 case, the NAG and FUC enzyme activity might be reflective of the absolute, but not relative
539 abundance of the mucin-degrading bacteria.

540 Since we found increased abundance of mucin-generalist bacteria and subsequently
541 increased mucin-degrading enzyme activity during the course of worm clearance, but not
542 during the course of worm retention, we questioned whether this is a result of underlying
543 qualitative changes in mucin production in goblet cells or whether a compensatory response to
544 increased mucin-foraging leads to qualitative changes in mucin secretion. To better understand
545 the changes in mucin secretion, we performed blinded counting of goblet cells in small (~0.5
546 cm) pieces of cecal tissue that were preserved in methacarn fixative. The goblet cell counts
547 revealed no significant changes in numbers throughout the experiment **(Fig. 5B)**. Furthermore,
548 the expression of neither the gene *Muc2* nor the gene *Muc5ac*, which play an important role in
549 worm clearance[62], were upregulated **(Tables S1–S3)**. However, since these transcripts do not
550 necessarily reflect protein production, involvement of these mucins and/or other mechanisms
551 (such as epithelial cell turnover), that contribute to host protection, cannot be ruled out.

552 Among the genes involved in the five most upregulated pathways in resistant mice, we
553 identified several genes involved in glycoprotein synthesis and glycosylation **(Fig. 5C)**. This

554 is especially interesting as many of the upregulated genes are involved in the glycosylation of
555 the colonic mucins[32,63,64]. For example, the expression of the glycosyltransferases *Fut2*,
556 *St3gal6*, *C1galt1*, *Galnt3* and *Galnt4* or the sulfotransferase *Gal3st2* were upregulated in the
557 resistant mice[32,63,64] **(Fig. 5C)**. Altered mucin glycosylation, in particular sulfation, has been
558 linked to modified *T. muris* susceptibility[64]. Thus, altered glycosylation might be responsible
559 for the improved clearance of *T. muris* in resistant mice. This is particularly intriguing
560 considering that the microbiome has a major influence on the glycosylation of the Muc2
561 glycoprotein, the major constituent of the colonic mucus layer[63]. Furthermore, enhanced
562 microbial mucin foraging could potentially increase interaction of the gut microbiome with the
563 host mast cells, which could explain the observed increase in MCPT1 **(Fig. 3E)**. Altogether,
564 our results suggest that the increased mucolytic activity of the gut microbiome under fiber
565 deprivation (**Fig. 5A)** without the compensatory mucin production **(Fig. 5B)**, but with possible
566 changes in mucin glycosylation **(Fig. 5C)**, aids in clearance of *T. muris*.
567

568 **Discussion**

569 Helminth infection models have been profoundly utilized to elucidate the underlying host
570 responses for the past several decades, yet open questions remain about the mechanisms of how
571 the intricate interactions between the gut microbiome and GI mucus affect worm infection
572 dynamics including the host immune responses. Here, we shed insight into the role of bacterial
573 mucin foraging in altering the host immune responses during the infection with *T. muris*. Using
574 a diet reduced in fiber to increase bacterial mucin foraging in a gnotobiotic mouse model
575 containing a 14-member synthetic human gut microbiota, our study supports a model in which
576 the increased microbial mucolytic activity promotes Th2-driven worm clearance **(Fig. 6)**. Our
577 results document an intricate link in the gut microbiome–parasite axis, suggesting a potential
578 mechanism through which increased microbial mucin foraging could alter the host immune
579 response to the worm.

580 Our study demonstrates that an IFNγ-dominated Th1 response, which has been shown
581 to drive chronic *T. muris* infections, is characterized by a balanced fiber vs. mucin degradation,
582 while successful clearance of the worm characterized by a type 2 response is potentially the
583 result of increased microbial mucin foraging during worm infection **(Figs. 2, 3 and 6)**. A recent
584 study by Myhill et al.[27] observed a similar IFNγ-driven shift from a Th2 toward a Th1 response
585 when feeding SPF mice a high-fiber diet containing 10% inulin, however, this study did not
586 provide an explanation for the underlying mechanisms. Using our 14SM model, a standard

587 mouse chow containing 3.8% dietary fiber and a diet deprived of fiber, we offer an explanation
588 that the mucin–microbiome interactions driven by dietary changes alter the host immune
589 responses and the worm infection dynamics **(Fig. 6)**. Despite the well-known specificity of
590 parasites for their hosts, it is clear that *T. muris* is able to establish and develop in the intestine
591 colonized by the synthetic, human 14SM for at least 30 days. It is well known that bacteria are
592 important for *T. muris* worm hatching[9,10], although the specific bacterial members involved are
593 not well known and it is possible that the selected bacteria in our synthetic human microbiota
594 might not be ideal for inducing egg hatching, resulting in a lower level of infection than would
595 normally be seen in SPF mice with a natural microflora. The system used here, however, does
596 provide a chronic low-level infection characteristic of infections under natural conditions.

597 *T. muris* has been shown to broadly alter the host's gut microbiome composition[23–28],
598 but our longitudinal characterization of the gut microbiome provides explicit details about how
599 the microbial shifts are characterized by distinct phases and specific microbial species based
600 on their functional roles **(Fig. 6)**. In resistant mice, the microbial functional changes during the
601 worm infection and clearance are largely centered around microbial mucin foraging. During
602 the early larval stages (L2–L3) around 13 to 15 DPI, we observed a major disruption of the gut
603 microbiome composition, especially in the FF-fed group **(Fig. 4)**, which was characterized by
604 a drastic expansion of *E. coli* on both diets as well as a decline of *A. muciniphila* in resistant
605 mice. A similar expansion of *Enterobacteriaceae* (*E. coli*) and decline of *Akkermansia* (*A.*
606 *muciniphila*) was observed following a high-dose infection of SPF mice fed an inulin-
607 supplemented diet[27]. The second major shift in microbial abundances occurs around 20 to 25
608 DPI which coincides with the moulting of the worm from the L3 to the L4 larval stage **(Fig.**
609 **4)**. During this transition, the worm moves to occupy cells nearer to the top of the crypt,
610 protruding into the lumen, thus most likely increasing its interaction with the gut microbiome[3].
611 In resistant mice, this shift is characterized by an increased abundance of the mucin generalists
612 *B. caccae* and *B. thetaiotaomicron*, resulting in an overall increased mucolytic activity of the
613 gut microbiome **(Figs. 4, 5A and 6)**. It is likely that the resulting secretion of M60-like
614 proteases by mucin generalists and the *T. muris*-secreted serine proteases depolymerize the
615 mucin backbone[21,31,32] generating new niches for other bacteria. This is reflected by the
616 increased abundance of *D. piger*, which forages the released sulfate and the increased
617 abundance of a strict fiber-degrader *E. rectale*, which can degrade the released mucin
618 monosaccharides.

619 In contrast to the observations in *Muc2*$^{-/-}$ mice[29], in our model, increased microbial
620 mucin foraging under fiber-deprived conditions did not delay the parasite clearance, but instead
621 promoted the clearance. These results are not unexpected as genetic ablation of Muc2 largely
622 destabilizes the mucus structure, whereas the increased microbial mucin foraging seems to
623 either resist transition to a Th1 response and/or aids in a Th2 response. We could not detect an
624 increase in goblet cell numbers/mucin production associated with this **(Fig. 5**B**)**. Nevertheless,
625 we observed increased transcription of genes involved in mucin glycosylation **(Fig. 5C)**, which
626 has been shown previously to alter susceptibility to *T. muris*[64]. Considering that the microbiome
627 can directly influence mucin glycosylation[63], our results suggest that the fiber-deprived diet-
628 induced changes in the microbiome might lead to an alteration in the glycosylation of the GI
629 mucins, which aids in clearance of *T. muris*. One caveat being that the gene transcription was
630 not assessed longitudinally, thus limiting interpretations considering the infection dynamics.
631 However, even if indirectly assessed, these data support the hypothesis that excessive mucin
632 degradation leads to closer interaction of the gut microbiome and the host mast cells, leading
633 to their activation or accumulation, as evidenced by an increase in MCPT1 concomitant with
634 worm clearance **(Figs. 3E and 6)**. Mast cells have been linked to *T. muris* clearance[56] and based
635 on the work with another nematode—*Trichinella spiralis*—this might be related to a mast cell-
636 dependent increase in epithelial permeability[65]. Therefore, an increase in MCPT1 offers an
637 additional explanation as to why excessive mucin foraging renders mice resistant to *T. muris*
638 infection. Finally, mast cell activation suppresses Th1 responses by decreasing IFNγ expression
639 and increasing Th2 cytokine expression[55], which offers an additional explanation how
640 excessive foraging of mucin could alter the host immune response. However, it is also likely
641 that the strong IFNγ expression on the FR diet simply impairs the type 2 and later mast cell
642 response.

643 Given the high morbidity associated with the parasitic infections in humans[1], our study
644 has generated important prerequisite knowledge for clinical settings: 1) for treating parasitic
645 infections – in the absence of co-infections, periodic fiber deprivation or fasting to boost
646 microbial mucin foraging could be potentially employed in the clinic to manage worm
647 infections; and 2) for harnessing the immunomodulatory properties of helminths for their
648 potential therapeutic use in inflammatory disorders[66] or allograft rejection[67]. Further research
649 is required about how the model proposed in our study **(Fig. 6)** could be translated into the
650 clinic.

651 **References**

652 1. World Health Organization. Global Health Estimates 2020: Disease burden by Cause,
653 Age, Sex, by Country and by Region, 2000-2019. 2020.

654 2. Douglas B, Oyesola O, Cooper MM, et al. Immune System Investigation Using
655 Parasitic Helminths. Annu Rev Immunol 2021;39:639–665.

656 3. Klementowicz JE, Travis MA, Grencis RK. Trichuris muris: A model of
657 gastrointestinal parasite infection. Semin Immunopathol 2012;34:815–828.

658 4. Yousefi Y, Haq S, Banskota S, et al. Trichuris muris model: Role in understanding
659 intestinal immune response, inflammation and host defense. Pathogens 2021;10.

660 5. Colombo SAP, Grencis RK. Immunity to Soil-Transmitted Helminths: Evidence From
661 the Field and Laboratory Models. Front Immunol 2020;11.

662 6. Zaiss MM, Harris NL. Interactions between the intestinal microbiome and helminth
663 parasites. Parasite Immunol 2016;38:5–11.

664 7. Brosschot TP, Reynolds LA. The impact of a helminth-modified microbiome on host
665 immunity review-article. Mucosal Immunol 2018;11:1039–1046.

666 8. Jaenike J, Unckless R, Cockburn SN, et al. Adaptation via symbiosis: Recent spread of
667 a drosophila defensive symbiont. Science (80-) 2010;329:212–215.

668 9. Hayes KS, Bancroft AJ, Goldrick M, et al. Exploitation of the intestinal microflora by
669 the parasitic nematode trichuris muris. Science (80-) 2010;328:1391–1394.

670 10. White EC, Houlden A, Bancroft AJ, et al. Manipulation of host and parasite
671 microbiotas: Survival strategies during chronic nematode infection. Sci Adv 2018;4.

672 11. Hewitson JP, Harcus Y, Murray J, et al. Proteomic analysis of secretory products from
673 the model gastrointestinal nematode Heligmosomoides polygyrus reveals dominance
674 of Venom Allergen-Like (VAL) proteins. J Proteomics 2011;74:1573–1594.

675 12. Abner SR, Parthasarathy G, Hill DE, et al. Trichuris suis: Detection of antibacterial
676 activity in excretory-secretory products from adults. Exp Parasitol 2001;99:26–36.

677 13. Su L, Su CW, Qi Y, et al. Coinfection with an intestinal helminth impairs host innate
678 immunity against Salmonella enterica serovar typhimurium and exacerbates intestinal
679 inflammation in mice. Infect Immun 2014;82:3855–3866.

680 14. Fricke WF, Song Y, Wang AJ, et al. Type 2 immunity-dependent reduction of
681 segmented filamentous bacteria in mice infected with the helminthic parasite
682 Nippostrongylus brasiliensis. Microbiome 2015;3:40.

683 15. Forman RA, DeSchoolmeester ML, Hurst RJM, et al. The Goblet Cell Is the Cellular
684 Source of the Anti-Microbial Angiogenin 4 in the Large Intestine Post Trichuris muris
685 Infection. PLoS One 2012;7.

686 16. Shea-Donohue T, Sullivan C, Finkelman FD, et al. The Role of IL-4 in
687 Heligmosomoides polygyrus -Induced Alterations in Murine Intestinal Epithelial Cell
688 Function. J Immunol 2001;167:2234–2239.

689 17. Harris JB, Podolsky MJ, Bhuiyan TR, et al. Immunologic responses to Vibrio cholerae
690 in patients co-infected with intestinal parasites in Bangladesh. PLoS Negl Trop Dis
691 2009;3.

692 18. Kosik-Bogacka DI, Wojtkowiak-Giera A, Kolasa A, et al. Hymenolepis diminuta:
693 Analysis of the expression of Toll-like receptor genes and protein (TLR3 and TLR9) in
694 the small and large intestines of rats. Exp Parasitol 2014;145:61–67.

695 19. Zakeri A, Borji H, Haghparast A. Interaction Between Helminths and Toll-Like
696 Receptors: Possibilities and Potentials for Asthma Therapy. Int Rev Immunol
697 2016;35:219–248.

698 20. Marillier RG, Michels C, Smith EM, et al. IL-4/IL-13 independent goblet cell
699 hyperplasia in experimental helminth infections. BMC Immunol 2008;9.

700 21. Hasnain SZ, McGuckin MA, Grencis RK, et al. Serine Protease(s) Secreted by the
701 Nematode Trichuris muris Degrade the Mucus Barrier. PLoS Negl Trop Dis 2012;6.

702 22. Hasnain SZ, Evans CM, Roy M, et al. Muc5ac: A critical component mediating the
703 rejection of enteric nematodes. J Exp Med 2011;208:893–900.

704 23. Li RW, Wu S, Li W, et al. Alterations in the porcine colon microbiota induced by the
705 gastrointestinal nematode Trichuris suis. Infect Immun 2012;80:2150–2157.

706 24. Broadhurst MJ, Ardeshir A, Kanwar B, et al. Therapeutic Helminth Infection of
707 Macaques with Idiopathic Chronic Diarrhea Alters the Inflammatory Signature and
708 Mucosal Microbiota of the Colon. PLoS Pathog 2012;8.

709 25. Holm JB, Sorobetea D, Kiilerich P, et al. Chronic Trichuris muris infection decreases
710 diversity of the intestinal microbiota and concomitantly increases the abundance of
711 lactobacilli. PLoS One 2015;10.

712 26. Houlden A, Hayes KS, Bancroft AJ, et al. Chronic Trichuris muris infection in
713 C57BL/6 mice causes significant changes in host microbiota and metabolome: Effects
714 reversed by pathogen clearance. PLoS One 2015;10.

715 27. Myhill LJ, Stolzenbach S, Mejer H, et al. Fermentable Dietary Fiber Promotes
716 Helminth Infection and Exacerbates Host Inflammatory Responses. J Immunol
717 2020;204:3042–3055.

718 28. Rosa BA, Snowden C, Martin J, et al. Whipworm-Associated Intestinal Microbiome
719 Members Consistent Across Both Human and Mouse Hosts. Front Cell Infect
720 Microbiol 2021;11.

721 29. Hasnain SZ, Wang H, Ghia JE, et al. Mucin Gene Deficiency in Mice Impairs Host
722 Resistance to an Enteric Parasitic Infection. Gastroenterology 2010;138:1763-1771.e5.

723 30. Johansson MEV, Jakobsson HE, Holmén-Larsson J, et al. Normalization of host
724 intestinal mucus layers requires long-term microbial colonization. Cell Host Microbe
725 2015;18:582–592.

726 31. Desai MS, Seekatz AM, Koropatkin NM, et al. A Dietary Fiber-Deprived Gut
727 Microbiota Degrades the Colonic Mucus Barrier and Enhances Pathogen
728 Susceptibility. Cell 2016;167:1339-1353.e21.

729 32. Martens EC, Neumann M, Desai MS. Interactions of commensal and pathogenic
730 microorganisms with the intestinal mucosal barrier. Nat Rev Microbiol 2018;16:457–
731 470.

732 33. Parrish A, Boudaud M, Kuehn A, et al. Intestinal mucus barrier: a missing piece of the
733 puzzle in food allergy. Trends Mol Med 2022;28:36–50.

734 34. Neumann M, Steimle A, Grant ET, et al. Deprivation of dietary fiber in specific-
735 pathogen-free mice promotes susceptibility to the intestinal mucosal pathogen
736 Citrobacter rodentium. Gut Microbes 2021;13.

737 35. Steimle A, Sciscio A De, Neumann M, et al. Constructing a gnotobiotic mouse model
738 with a synthetic human gut microbiome to study host–microbe cross talk. STAR

739 Protoc 2021;2:100607.

740 36. Wakelin D. Acquired immunity to Trichuris muris in the albino laboratory mouse.
741 Parasitology 1967;57:515–524.

742 37. Hayes KS, Cliffe LJ, Bancroft AJ, et al. Chronic Trichuris muris infection causes
743 neoplastic change in the intestine and exacerbates tumour formation in APC min/+
744 mice. PLoS Negl Trop Dis 2017;11.

745 38. Steimle A, Grant ET, Desai MS. Quantitative assay to detect bacterial glycan-
746 degrading enzyme activities in mouse and human fecal samples. STAR Protoc
747 2021;2:100326.

748 39. Martin M. Cutadapt removes adapter sequences from high-throughput sequencing
749 reads. EMBnet.journal 2011;17:10.

750 40. Dobin A, Davis CA, Schlesinger F, et al. STAR: Ultrafast universal RNA-seq aligner.
751 Bioinformatics 2013;29:15–21.

752 41. Anders S, Huber W. Differential expression analysis for sequence count data. Genome
753 Biol 2010;11.

754 42. Love MI, Huber W, Anders S. Moderated estimation of fold change and dispersion for
755 RNA-seq data with DESeq2. Genome Biol 2014;15.

756 43. Yu G, Wang LG, Han Y, et al. ClusterProfiler: An R package for comparing biological
757 themes among gene clusters. Omi A J Integr Biol 2012;16:284–287.

758 44. Supek F, Bošnjak M, Škunca N, et al. Revigo summarizes and visualizes long lists of
759 gene ontology terms. PLoS One 2011;6.

760 45. Wolter M, Steimle A, Parrish A, et al. Dietary Modulation Alters Susceptibility to
761 Listeria monocytogenes and Salmonella Typhimurium with or without a Gut
762 Microbiota. mSystems 2021;6:e00717-21.

763 46. Chassaing B, Srinivasan G, Delgado MA, et al. Fecal Lipocalin 2, a Sensitive and
764 Broadly Dynamic Non-Invasive Biomarker for Intestinal Inflammation Bereswill S,
765 ed. PLoS One 2012;7:e44328.

766 47. Zhao P, Elks CM, Stephens JM. The induction of lipocalin-2 protein expression in
767 vivo and in vitro. J Biol Chem 2014;289:5960–5969.

768 48. Chaudhuri A. Regulation of macrophage polarization by RON receptor tyrosine kinase
769 signaling. Front Immunol 2014;5.

770 49. Forman R, Logunova L, Smith H, et al. Trichuris muris infection drives cell-intrinsic
771 IL4R alpha independent colonic RELMα+ macrophages. PLoS Pathog 2021;17.

772 50. Sorobetea D, Svensson-Frej M, Grencis R. Immunity to gastrointestinal nematode
773 infections. Mucosal Immunol 2018;11:304–315.

774 51. Hallowell RW, Collins SL, Craig JM, et al. MTORC2 signalling regulates M2
775 macrophage differentiation in response to helminth infection and adaptive
776 thermogenesis. Nat Commun 2017;8.

777 52. Deschoolmeester ML, Else KJ. Cytokine and chemokine responses underlying acute
778 and chronic Trichuris muris infection. Int Rev Immunol 2002;21:439–467.

779 53. Else KJ, Entwistle GM, Grencis RK. Correlations between worm burden and markers
780 of Th1 and Th2 cell subset induction in an inbred strain of mouse infected with
781 Trichuris muris. Parasite Immunol 1993;15:595–600.

782 54. Kasakura K, Nagata K, Miura R, et al. Cooperative Regulation of the Mucosal Mast
783 Cell–Specific Protease Genes Mcpt1 and Mcpt2 by GATA and Smad Transcription
784 Factors. J Immunol 2020;204:1641–1649.

785 55. Mazzoni A, Siraganian RP, Leifer CA, et al. Dendritic Cell Modulation by Mast Cells
786 Controls the Th1/Th2 Balance in Responding T Cells. J Immunol 2006;177:3577–
787 3581.

788 56. Hayes KS, Grencis RK. Trichuris muris and comorbidities-within a mouse model
789 context. Parasitology 2021;148:1774–1782.

790 57. Hayes KS, Hager R, Grencis RK. Sex-dependent genetic effects on immune responses
791 to a parasitic nematode. BMC Genomics 2014;15.

792 58. Browne HP, Neville BA, Forster SC, et al. Transmission of the gut microbiota:
793 Spreading of health. Nat Rev Microbiol 2017;15:531–543.

794 59. Luis AS, Jin C, Pereira GV, et al. A single sulfatase is required to access colonic
795 mucin by a gut bacterium. Nature 2021;598:332–337.

796 60. Rey FE, Gonzalez MD, Cheng J, et al. Metabolic niche of a prominent sulfate-

797 reducing human gut bacterium. Proc Natl Acad Sci U S A 2013;110:13582–13587.

798 61. Rogers TE, Pudlo NA, Koropatkin NM, et al. Dynamic responses of Bacteroides
799 thetaiotaomicron during growth on glycan mixtures. Mol Microbiol 2013;88:876–890.

800 62. Larsson JMH, Thomsson KA, Rodríguez-Piñeiro AM, et al. Studies of mucus in
801 mouse stomach, small intestine, and colon. III. Gastrointestinal Muc5ac and Muc2
802 mucin O-glycan patterns reveal a regiospecific distribution. Am J Physiol -
803 Gastrointest Liver Physiol 2013;305.

804 63. Arike L, Holmén-Larsson J, Hansson GC. Intestinal Muc2 mucin O-glycosylation is
805 affected by microbiota and regulated by differential expression of glycosyltranferases.
806 Glycobiology 2017;27:318–328.

807 64. Hasnain SZ, Dawson PA, Lourie R, et al. Immune-driven alterations in mucin
808 sulphation is an important mediator of Trichuris muris helminth expulsion. PLoS
809 Pathog 2017;13.

810 65. McDermott JR, Bartram RE, Knight PA, et al. Mast cells disrupt epithelial barrier
811 function during enteric nematode infection. Proc Natl Acad Sci U S A 2003.

812 66. Helmby H. Human helminth therapy to treat inflammatory disorders- where do we
813 stand? BMC Immunol 2015;16.

814 67. Kiss M, Burns H, Donnelly S, et al. Effectiveness of Helminth Therapy in the
815 Prevention of Allograft Rejection: A Systematic Review of Allogeneic
816 Transplantation. Front Immunol 2020;11.

817 **Figure legends**

818 **Figure 1. Diet drives changes in mucin-degrading bacteria and alters worm infection.** (A)
819 Experimental timeline. Age-matched 18–23 weeks old germ-free (GF) C57BL/6 mice were
820 gavaged with the synthetic 14-member gut microbiota (14SM) on two consecutive days. These
821 colonized mice were maintained for six days on the fiber-rich (FR) diet, after which nearly half
822 of the mice were switched to a fiber-free (FF) diet. The mice were maintained for 20 days on
823 their respective diets, after which they were gavaged with *T. muris* eggs. The infection was
824 observed for up to 30 days and on day 13, 15, 20, 25 and 30 post infection 4–5 mice were
825 euthanized for final readouts. (B) Relative bacterial abundance at day 0, just before the
826 infection, determined by qPCR on DNA extracted from fecal pellets. Red latin crosses denote
827 known mucin-degrading bacteria. (C) Weekly assessed weights of *T. muris* infected mice. Error
828 bars represent SEM and significance labels comparisons between FR and FF group as
829 determined by an unpaired, two-tailed t-test. (D) Worm burdens assessed on the mice
830 euthanized at day 13, 15, 20, 25 and 30 post infection. Error bars represent SEM; unpaired,
831 two-tailed t-test. (E) Fecal Lipocalin-2 (LCN-2) levels assessed by ELISA before (day 0) and
832 after infection with *T. muris* (13, 15, 20, 23, 30 DPI). Error bars represent SEM; unpaired t-
833 test. ns, non-significant; *$p<0.05$; **$p<0.01$; ***$p<0.001$; ****$p<0.0001$.
834

835 **Figure 2. Host transcriptomics supports chronic and acute outcome of worm infection.**
836 Analysis of data generated by RNA-seq of RNA extracted from colonic tissue at day 30 post
837 infection (n = 4 per group). (A) Volcano plot of the distribution of all differentially expressed
838 genes. (B) Barplot showing significantly up- or downregulated host pathways (Fiber Rich
839 (FR)/Fiber Free (FF)) determined by Ingenuity Pathway Analysis (IPA). The higher the opacity
840 of the bar, the more up- or downregulated the pathway. (C) Graphical summary generated by
841 IPA showing the major upregulated genes and pathways as well as their interactions.
842

843 **Figure 3. Maintenance or moderate increase of Th2 immunity leads to worm expulsion.**
844 (A) Relative cytokine expression of INFγ, IL-04 and IL-13 (Fiber-free versus Fiber-rich fed
845 mice) determined by qPCR using RNA extracted from mesenteric lymph nodes and colonic
846 tissue (colon) at 30 days post infection (n = 3-5). Error bars represent 95% confidence intervals;
847 unpaired, two-tailed t-test. (B) Serum cytokine concentrations determined by LEGENDplex
848 bead-based immunoassay at days 30 post infection. Error bars represent SEM; unpaired, two-
849 tailed t-test. (C) Total IgE and total IgG1 concentrations determined by ELISA on mouse

850 serum. Error bars represent SEM; two-way ANOVA using a Šidák multiple comparison test.
851 (D) Parasite-specific IgG1 and IgG2c concentrations determined by ELISA on mouse serum.
852 Error bars represent SEM; two-way ANOVA using a Šidák multiple comparison test. (E)
853 Serum mast cell protease 1 (MCPT1) concentrations determined by ELISA. Error bars
854 represent SEM. Black significance labels denote comparisons between FR and FF groups. Red
855 asterisk denotes significant comparison to day 0 within the FF group. Error bars represent SEM;
856 Two-way ANOVA using a Šidák multiple comparison test; ns, non-significant; *p<0.05;
857 **p<0.01; ***p<0.001; ****p<0.0001.
858
859 **Figure 4. Mucin-generalist bacteria increase during worm clearance.** (A) PCoA plot of the
860 microbiome composition of all mice split by diet (left panel) or by day and diet (middle and
861 right panels). PCs were selected based on Eigenvalues. (B) Microbial composition of the gut
862 microbiota before the infection (day 0) and at day 13, 15, 20, 25 and 30 post infection (denoted
863 by dotted lines). Relative bacterial abundances were determined by qPCR of DNA extracted
864 from fecal pellets using primers specific to each bacterial strain. Red crosses denote known
865 mucin-degrading bacteria. (C) Relative abundances of individual bacterial strains. Black
866 significance labels denote comparisons between the Fiber-rich (FR) and Fiber-free (FF) groups
867 on a specific day. Green asterisks denote significant comparisons to day 0 within the FR group.
868 Red asterisks similarly denote significant comparisons to day 0 within the FF group. Error bars
869 represent SEM; two-way ANOVA using a Šidák multiple comparison test. (D) Fold-change of
870 mucin generalists (*Bacteroides caccae* and *Bacteroides thetaiotaomicron*) and mucin
871 specialists *(Akkermansia muciniphila* and *Barnesiella intestinihominis*) normalized by their
872 average day 0 relative abundance. Black significance labels denote comparisons between the
873 FR and FF group on a specific day. Green asterisks denote significant comparisons to day 0
874 within the FR group. Red asterisks similarly denote significant comparisons to day 0 within
875 the FF group. Error bars represent SEM; two-way ANOVA using a Šidák multiple comparison
876 test. ns, non-significant; *p<0.05; **p<0.01; ***p<0.001; ****p<0.0001.
877
878 **Figure 5. Increased mucin–microbiome interactions promote worm clearance.** (A)
879 Glycan-degrading enzyme activities of the gut microbiome determined by stool-based p-
880 nitrophenyl glycoside-based enzyme assays. β-N-acetyl-glucosaminidase (NAG) and α-
881 fucosidase (FUC) are key mucin-degrading enzymes, while β-glucosidase (GLUC) serves as a
882 control for general glycan-degrading activity. Error bars represent SEM; Mann-Whitney test
883 between Fiber-rich (FR) and Fiber-free (FF) groups. (B) Goblet cell counts per crypt of *T.*

884 *muris* infected mice determined by histological assessment of methacarn-fixed cecum sections.
885 Error bars represent SEM; two-way ANOVA using a Šidák multiple comparison test. (C)
886 Relative gene expression (FF/FR) at 30 days post infection of the 5 most significant activated
887 pathways in the colonic tissue under FF conditions (n = 4 per group). Pathways are based on
888 GO terms for biological processes and REVIGO was used to reduce redundant terms. ns, non-
889 significant; *p<0.05; **p<0.01. †Adaptive immune response is based on somatic
890 recombination of immune receptors built from immunoglobulin superfamily domains.
891
892 **Figure 6. Model for clearance of *T. muris* following excessive microbial mucin foraging.**
893 Under homeostatic conditions there is a balance between bacterial fiber- and mucin-
894 degradation. Deprivation of dietary fiber leads to an increased bacterial mucin-degrading
895 activity of the gut microbiome, which is further increased after infection with *T. muris*. This
896 increase is a result of the expansion of mucin-generalist bacteria around 20 DPI, which in turn
897 opens up a growth niche for other bacteria such as *D. piger* and *E. rectale*, which can utilize
898 the sulfate or simple mucin glycoproteins, respectively, resulting from the depolymerization of
899 the complex host mucins by the mucin-generalist bacteria. In contrast to mucin-generalists,
900 mucin-specialists drastically drop in abundance following worm hatching in Fiber-free (FF)-
901 diet fed mice. In Fiber-rich (FR)-diet fed mice, the host develops a Th1 response characterized
902 by an increase of Th1-type cytokines, particularly IFNγ, and the production of parasite specific
903 IgG2 resulting in a chronic *T. muris* infection. In contrast, the excessive mucin foraging in FF-
904 fed mice leads to a moderate Th2 response characterized by the secretion of Th2 cytokines,
905 expression of parasite-specific IgG1 and increased degranulation of mast cells ultimately
906 leading to the clearance of *T. muris* around 30 DPI.

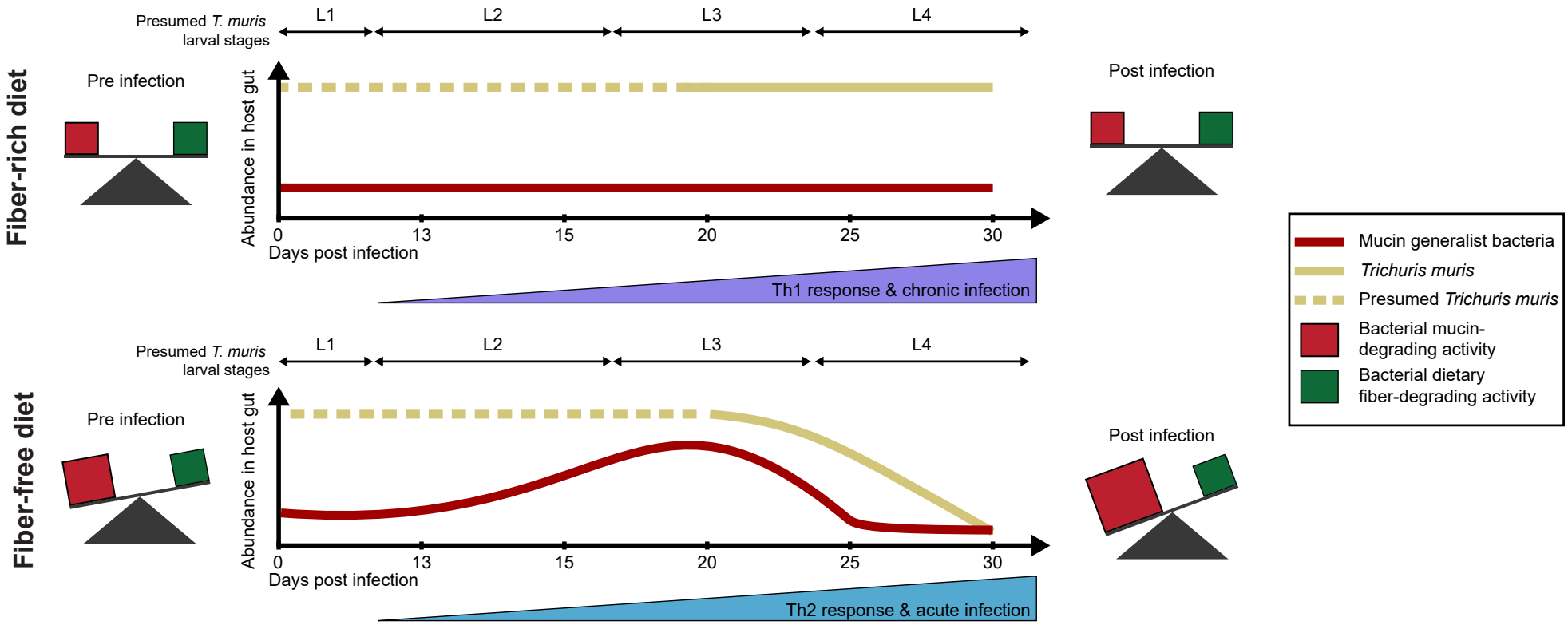

Graphical abstract

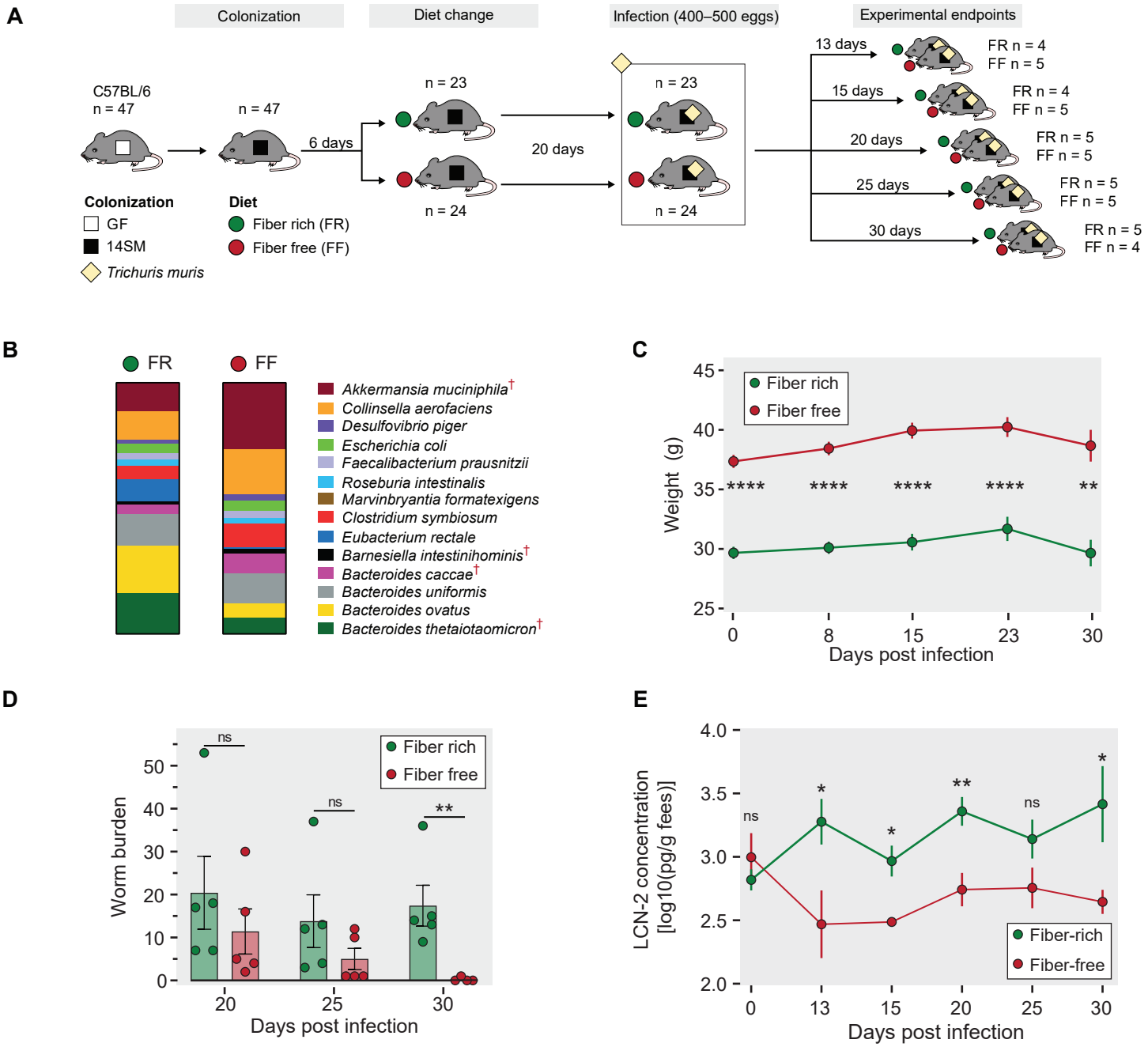
A
Colonization
Diet change
Infection (400–500 eggs)
Experimental endpoints
C57BL/6
n = 47
n = 47
6 days
n = 23
n = 24
20 days
n = 23
n = 24
13 days
15 days
20 days
25 days
30 days
FR n = 4
FF n = 5
FR n = 4
FF n = 5
FR n = 5
FF n = 5
FR n = 5
FF n = 5
FR n = 5
FF n = 4
Colonization
GF
14SM
Trichuris muris
Diet
Fiber rich (FR)
Fiber free (FF)
B
FR
FF
Akkermansia muciniphila†
Collinsella aerofaciens
Desulfovibrio piger
Escherichia coli
Faecalibacterium prausnitzii
Roseburia intestinalis
Marvinbryantia formatexigens
Clostridium symbiosum
Eubacterium rectale
Barnesiella intestinihominis†
Bacteroides caccae†
Bacteroides uniformis
Bacteroides ovatus
Bacteroides thetaiotaomicron†
C
Fiber rich
Fiber free
Weight (g)
45
40
35
30
25
****
****
****
****
**
0
8
15
23
30
Days post infection
D
Fiber rich
Fiber free
Worm burden
50
40
30
20
10
0
ns
ns
**
20
25
30
Days post infection
E
LCN-2 concentration
[log10(pg/g fees)]
4.0
3.5
3.0
2.5
2.0
ns
*
*
**
ns
*
Fiber-rich
Fiber-free
0
13
15
20
25
30
Days post infection

Figure 1

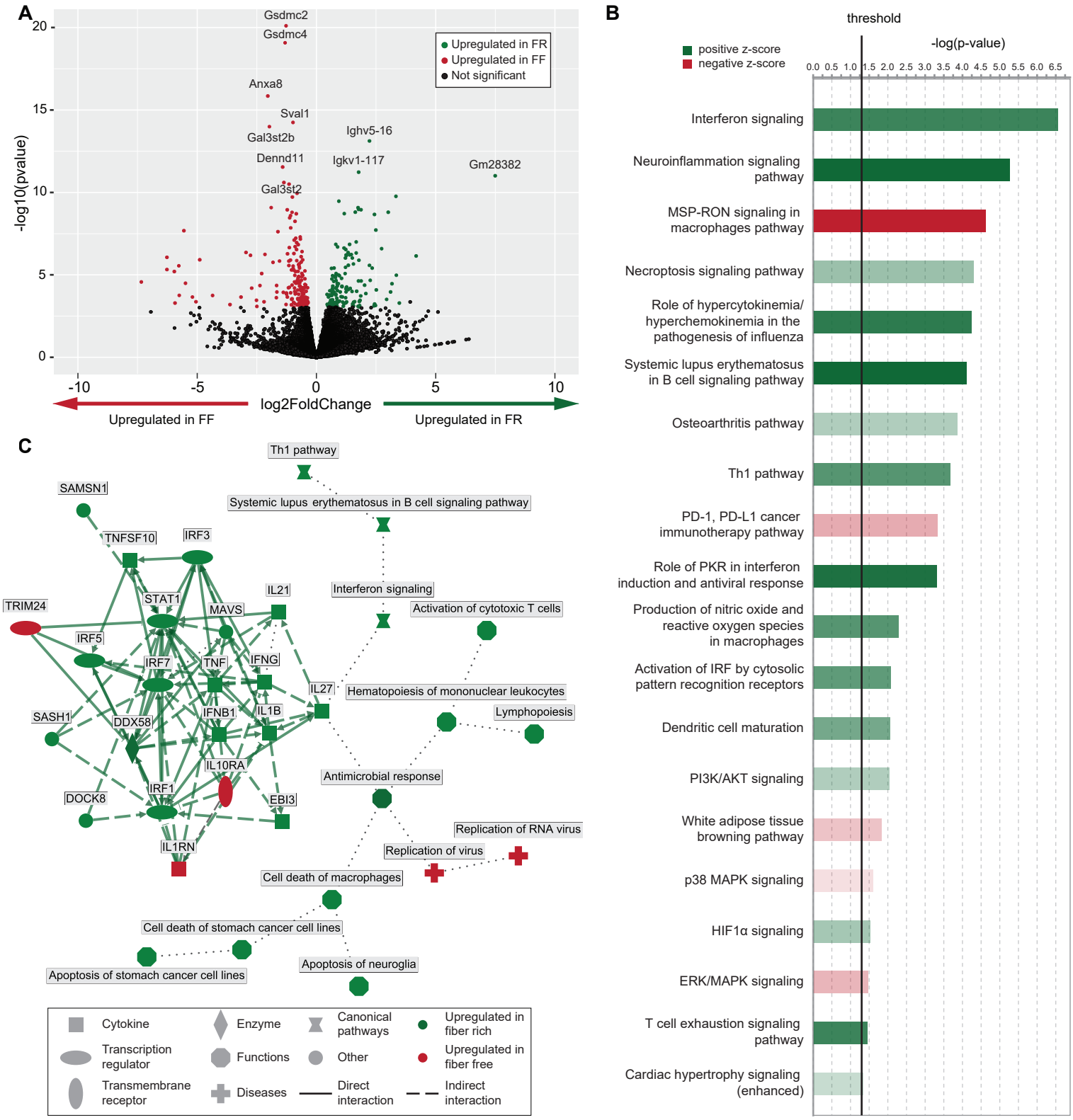
A
Gsdmc2
Gsdmc4
Anxa8
Sval1
Gal3st2b
Dennd11
Gal3st2
Ighv5-16
Igkv1-117
Gm28382
Upregulated in FR
Upregulated in FF
Not significant
-log10(pvalue)
log2FoldChange
Upregulated in FF
Upregulated in FR
B
threshold
positive z-score
negative z-score
-log(p-value)
Interferon signaling
Neuroinflammation signaling pathway
MSP-RON signaling in macrophages pathway
Necroptosis signaling pathway
Role of hypercytokinemia/ hyperchemokinemia in the pathogenesis of influenza
Systemic lupus erythematosus in B cell signaling pathway
Osteoarthritis pathway
Th1 pathway
PD-1, PD-L1 cancer immunotherapy pathway
Role of PKR in interferon induction and antiviral response
Production of nitric oxide and reactive oxygen species in macrophages
Activation of IRF by cytosolic pattern recognition receptors
Dendritic cell maturation
PI3K/AKT signaling
White adipose tissue browning pathway
p38 MAPK signaling
HIF1α signaling
ERK/MAPK signaling
T cell exhaustion signaling pathway
Cardiac hypertrophy signaling (enhanced)
C
Th1 pathway
Systemic lupus erythematosus in B cell signaling pathway
Interferon signaling
Activation of cytotoxic T cells
Hematopoiesis of mononuclear leukocytes
Lymphopoiesis
Antimicrobial response
Replication of RNA virus
Replication of virus
Cell death of macrophages
Cell death of stomach cancer cell lines
Apoptosis of stomach cancer cell lines
Apoptosis of neuroglia
SAMSN1
TNFSF10
IRF3
TRIM24
STAT1
MAVS
IL21
IRF5
IRF7
TNF
IFNG
IL27
SASH1
DDX58
IFNB1
IL1B
IL10RA
DOCK8
IRF1
EBI3
IL1RN
Cytokine
Enzyme
Canonical pathways
Upregulated in fiber rich
Transcription regulator
Functions
Other
Upregulated in fiber free
Transmembrane receptor
Diseases
Direct interaction
Indirect interaction

Figure 2

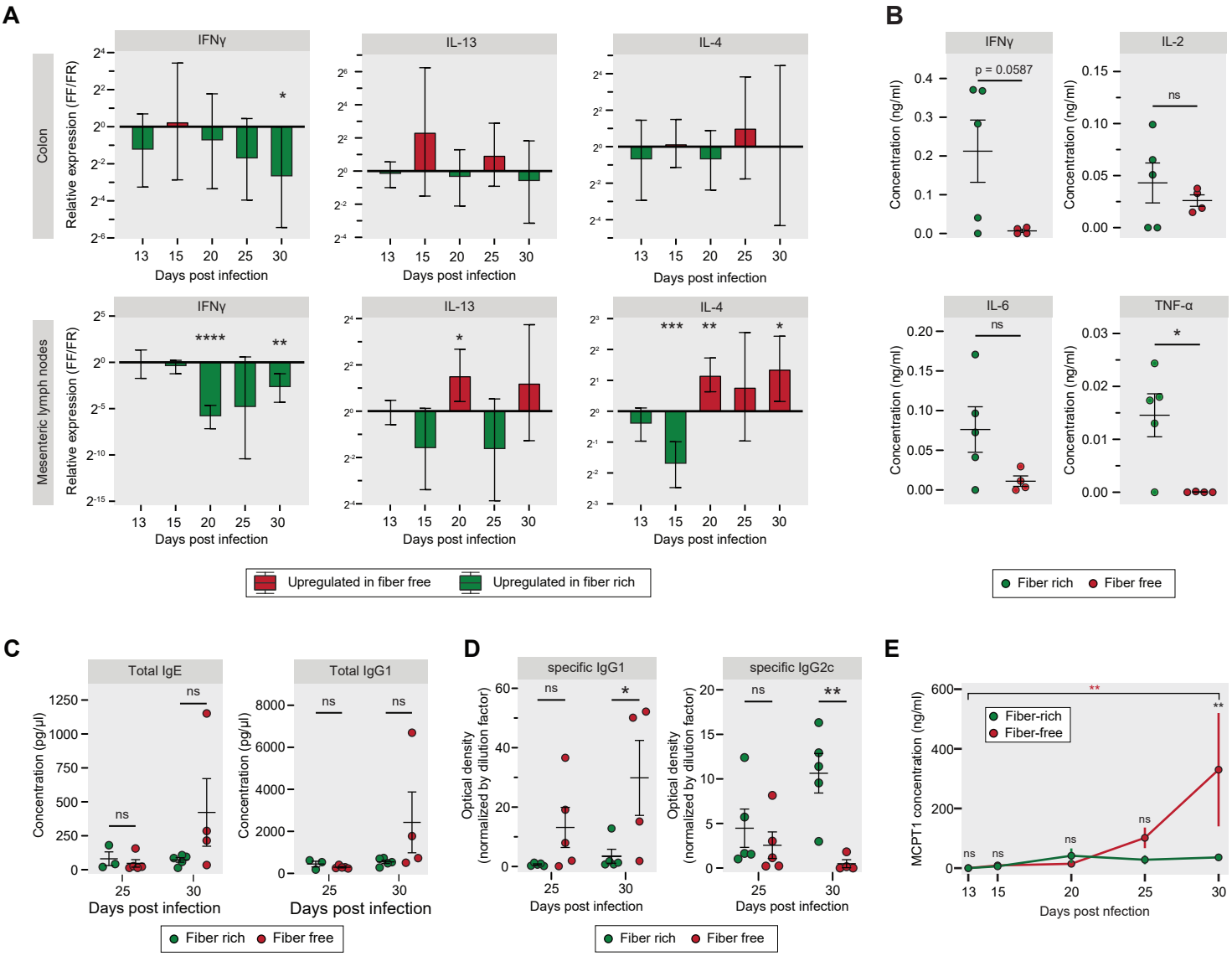
A
Colon
Mesenteric lymph nodes
IFNγ
IL-13
IL-4
Relative expression (FF/FR)
Days post infection
Upregulated in fiber free
Upregulated in fiber rich
B
IFNγ
IL-2
IL-6
TNF-α
Concentration (ng/ml)
p = 0.0587
ns
Fiber rich
Fiber free
C
Total IgE
Total IgG1
Concentration (pg/µl)
Days post infection
D
specific IgG1
specific IgG2c
Optical density (normalized by dilution factor)
E
MCPT1 concentration (ng/ml)
Fiber-rich
Fiber-free
Days post nfection

Figure 3

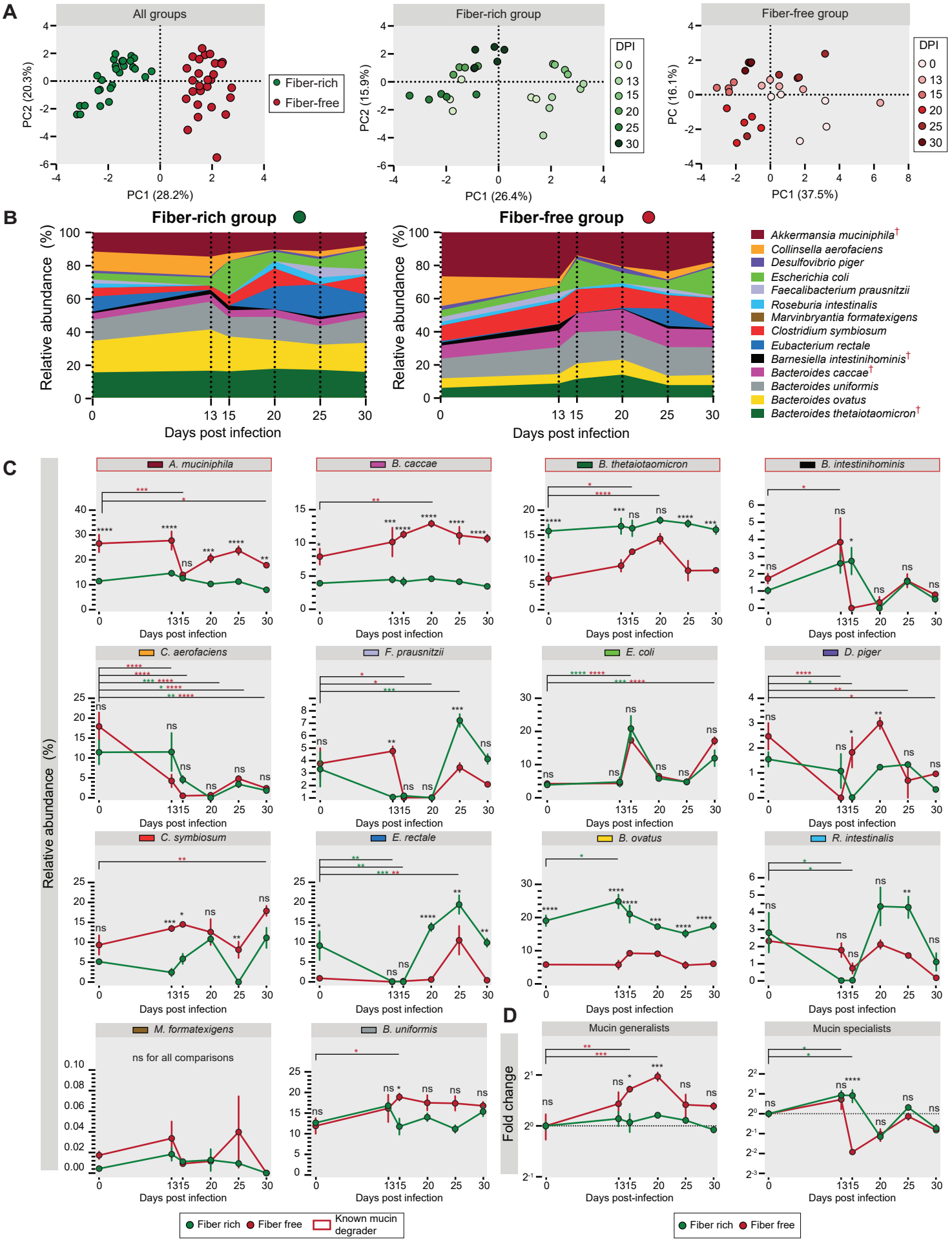
A
All groups
Fiber-rich group
Fiber-free group
Fiber-rich
Fiber-free
DPI
0
13
15
20
25
30
PC1 (28.2%)
PC2 (20.3%)
PC1 (26.4%)
PC2 (15.9%)
PC1 (37.5%)
PC (16.1%)
B
Fiber-rich group
Fiber-free group
Relative abundance (%)
Days post infection
Akkermansia muciniphila†
Collinsella aerofaciens
Desulfovibrio piger
Escherichia coli
Faecalibacterium prausnitzii
Roseburia intestinalis
Marvinbryantia formatexigens
Clostridium symbiosum
Eubacterium rectale
Barnesiella intestinihominis†
Bacteroides caccae†
Bacteroides uniformis
Bacteroides ovatus
Bacteroides thetaiotaomicron†
C
A. muciniphila
B. caccae
B. thetaiotaomicron
B. intestinihominis
C. aerofaciens
F. prausnitzii
E. coli
D. piger
C. symbiosum
E. rectale
B. ovatus
R. intestinalis
M. formatexigens
B. uniformis
ns for all comparisons
Relative abundance (%)
Days post infection
Fiber rich
Fiber free
Known mucin degrader
D
Mucin generalists
Mucin specialists
Fold change
Days post-infection
Fiber rich
Fiber free

Figure 4

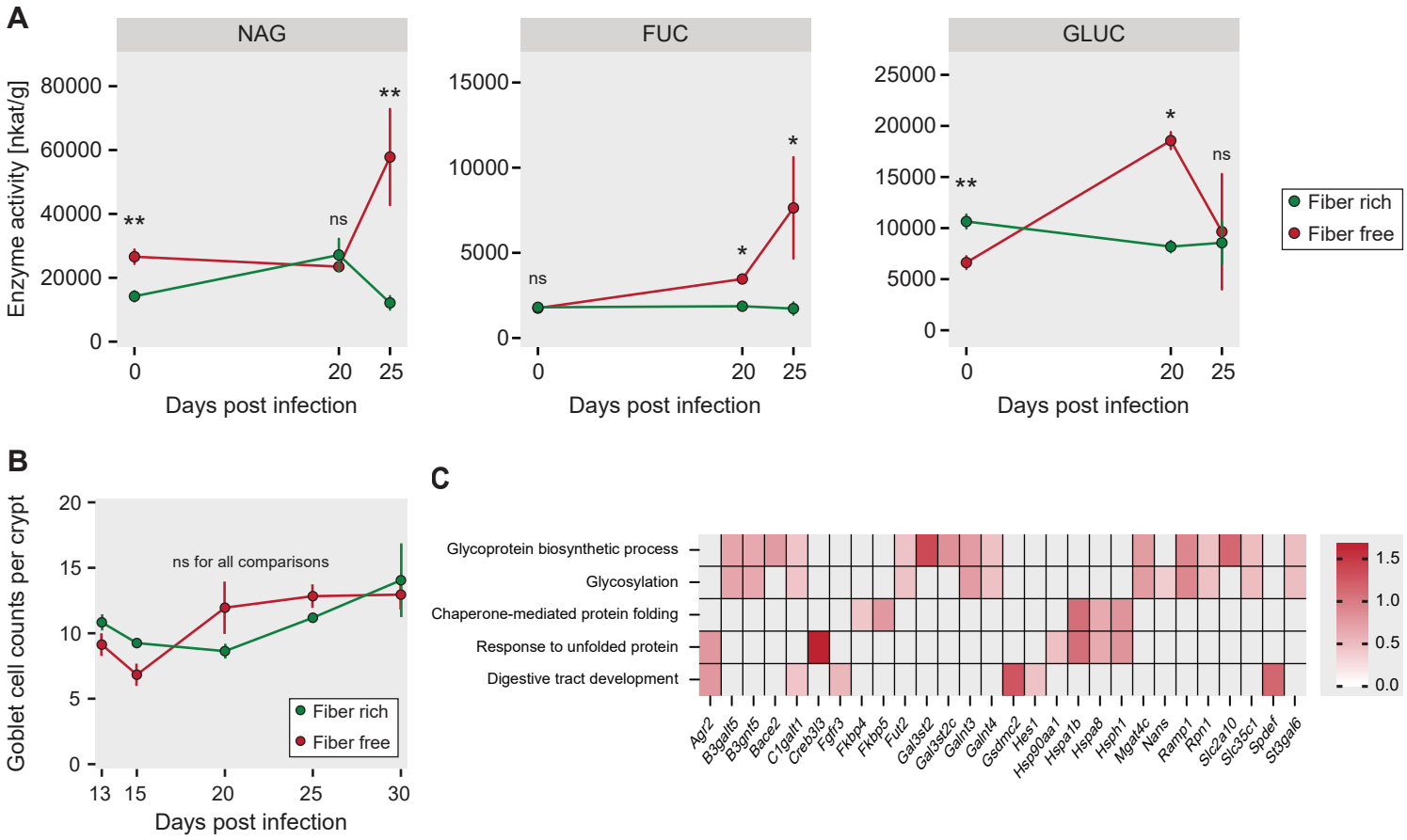
A
NAG
FUC
GLUC
Enzyme activity [nkat/g]
Days post infection
Fiber rich
Fiber free
ns
B
Goblet cell counts per crypt
ns for all comparisons
C
Glycoprotein biosynthetic process
Glycosylation
Chaperone-mediated protein folding
Response to unfolded protein
Digestive tract development
Agr2
B3galt5
B3gnt5
Bace2
C1galt1
Creb3l3
Fgfr3
Fkbp4
Fkbp5
Fut2
Gal3st2
Gal3st2c
Galnt3
Galnt4
Gsdmc2
Hes1
Hsp90aa1
Hspa1b
Hspa8
Hsph1
Mgat4c
Nans
Ramp1
Rpn1
Slc2a10
Slc35c1
Spdef
St3gal6

Figure 5

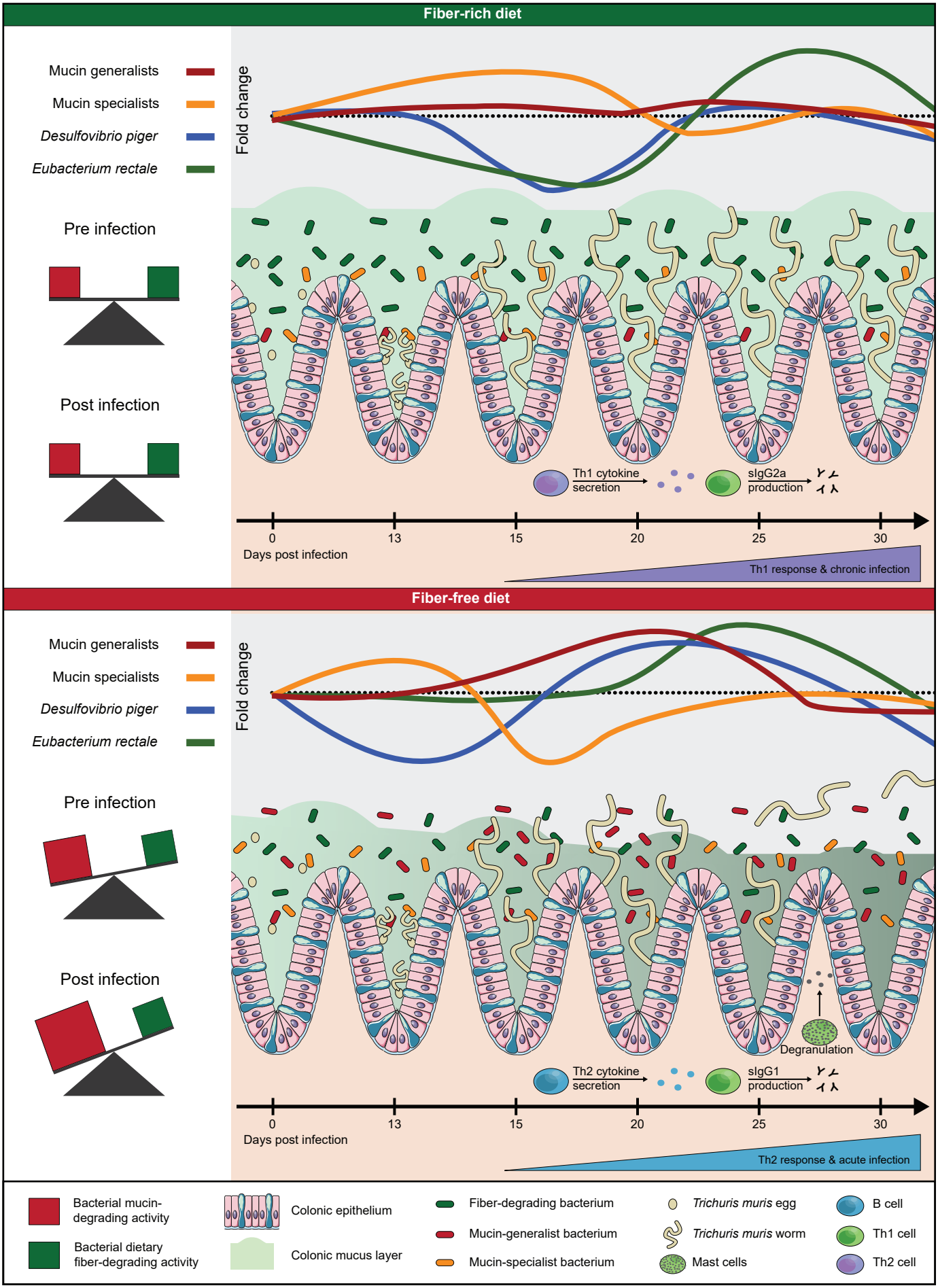
Fiber-rich diet
Mucin generalists
Mucin specialists
Desulfovibrio piger
Eubacterium rectale
Fold change
Pre infection
Post infection
Th1 cytokine secretion
sIgG2a production
0
13
15
20
25
30
Days post infection
Th1 response & chronic infection
Fiber-free diet
Mucin generalists
Mucin specialists
Desulfovibrio piger
Eubacterium rectale
Fold change
Pre infection
Post infection
Degranulation
Th2 cytokine secretion
sIgG1 production
0
13
15
20
25
30
Days post infection
Th2 response & acute infection
Bacterial mucin-degrading activity
Bacterial dietary fiber-degrading activity
Colonic epithelium
Colonic mucus layer
Fiber-degrading bacterium
Mucin-generalist bacterium
Mucin-specialist bacterium
Trichuris muris egg
Trichuris muris worm
Mast cells
B cell
Th1 cell
Th2 cell

Figure 6

Supplementary figure legends

Figure S1. Host gene expression on the FR diet is dominated by genes involved in Th1 response. Relative gene expression (FR/FF) at 30 days post infection of the 5 most significant activated pathways in the colonic tissue under FF conditions (n = 4 per group). Pathways are based on GO terms for biological processes and REVIGO was used to reduce redundant terms.

Figure S2. Cytokine transcript and protein abundances on different days post worm infection. (A) Relative cytokine expression of TNF-α, IL-5, IL-22 and IL-17a (fiber-free over fiber-rich fed mice) determined by qPCR of cDNA from RNA extracted from mesenteric lymph nodes (MLN) and colonic tissue (colon) at 13 and 30 DPI. Error bars represent 95% confidence intervals; unpaired, two-tailed t-test. (B) Serum cytokine concentrations of IL-22 and IL-5 at 30 DPI determined by LEGENDplex bead-based immunoassay. Error bars represent SEM; unpaired, two-tailed t-test. (C) Relative transcription factor expression of Tbet and GATA3 (Fiber-free over Fiber-rich fed mice) determined by qPCR using RNA extracted from mesenteric lymph nodes (MLN) and colonic tissue (colon) at 13–30 DPI. In the colon, GATA3 for all DPI and Tbet for 13 DPI were below the detection threshold. Error bars represent 95% confidence intervals; unpaired, two-tailed t-test; ns, non-significant; *$p<0.05$; **$p<0.01$.

Figure S3. Absolute abundances of cytokine transcripts on different days post worm infection. (A) Absolute cytokine and transcription factor expression as determined by qPCR using RNA extracted from mesenteric lymph nodes (MLN) and colonic tissue (colon) at 13, 15, 20, 25 and 30 DPI. Error bars represent SEM; unpaired, two-tailed t-test. (B) Absolute cytokine expression as determined by qPCR of using RNA extracted from mesenteric lymph nodes (MLN) and colonic tissue (colon) at 13 and 30 DPI. Error bars represent SEM; unpaired, two-tailed t-test. In the colon, GATA3 for all DPI and Tbet for 13 DPI were below the detection threshold. Error bars represent 95% confidence intervals; unpaired, two-tailed t-test; ns, non-significant; *$p<0.05$; **$p<0.01$; ***$p<0.001$; ****$p<0.0001$.

Supplementary table legends

Table S1. Relative gene expression (FR/FF) based differential expression analysis using DESeq2.

Table S2. Significantly upregulated pathways in FR diet based on gene oncology (GO) terms for biological processes.

Table S3. Significantly upregulated pathways in FF diet based on gene oncology (GO) terms for biological processes.

Table S4. RT-qPCR primers for genes encoding various cytokines, transcription factors and a reference (GAPDH).

Supplemental methods

Serum ELISA for total IgG1 and IgE

Serum ELISA for total IgG1 and IgE were performed as follows. Plate were coated overnight at room temperature using 0.5 µg/µl rat α mouse IgE purified UNLB (Imtec Diagnostics, 1130-01) or rat α-mouse IgG1 purified UNLB (Imtec Diagnostics, Ardmore, OK, United States; catalog no. 1144-01) capture antibody, respectively, diluted in 0.05 M carbonate/bicarbonate buffer (pH 9.6). Wells were washed three times using a washing buffer consisting of 1% Tween, 154 mM NaCl, 10 mM Trizma Base. 1% w/v of BSA in a TBS buffer (15 mM Trizma-acetate, 136 mM NaCl & 2 mM KCl) was used to block plates by incubating them for 2 hours at room temperature. Afterwards, plates were washed three times using the washing buffer. As controls, Mouse IgG1 Isotype Control UNLB (Imtec Diagnostics, Ardmore, OK, United States; catalog no 0102-01) or Mouse IgE Isotype Control (UNLB), Southern Biotech (Imtec Diagnostics, Ardmore, OK, United States; catalog no 0114-01) was used to generate two-fold serial dilutions. Serum samples were two-fold diluted from 1/40 to 1/1280 using the aforementioned TBS buffer with 0.1% w/v Tween-20 and 1% BSA. Plates were loaded the standards and samples were incubated for 90 minutes at room temperature. Another three wash steps were performed before loading a 1/500 dilution of the 2nd antibody, Goat anti-mouse IgG1-AP, Southern Biotech (Imtec diagnostics, Ardmore, OK, United States; catalog no 1071-04) or Goat anti-mouse IgE-AP, Southern Biotech (Imtec diagnostics, Ardmore, OK, United States; catalog no 1110-04), respectively. The final three wash steps were performed before loading the substrate solution consisting of 0.5 mg/ml phosphate substrate (Sigma-Aldrich, St. Louis, MO, United States; catalog no. S0642-200 TAB) in 1 mM AMP and 0.1 mM $MgCl_2 \cdot 6H_2O$. Plates were incubated for 1 hour at 37°C before they were read at 405 nm using a SpectraMax ABS PLUS spectrophotometer (Molecular Devices, San Jose, CA, United States).

RNA extraction from mesenteric lymph nodes and colonic tissue

Serum ELISA for total IgG1 and IgE were performed as follows. Plate were coated overnight at room temperature using 20 µl/well of 0.5 µg/µl rat α mouse IgE purified UNLB (Imtec Diagnostics, 1130-01) or rat α-mouse IgG1 purified UNLB (Imtec Diagnostics, Ardmore, OK, United States; catalog

no. 1144-01) capture antibody, respectively, diluted in 0.05 M carbonate/bicarbonate buffer at pH 9.6. Wells were washed three times using 100 µl/well of a washing buffer consisting of 1% Tween, 154 mM NaCl, 10 mM Trizma Base. Then plates were blocked by incubating them for 2 hours at room temperature with 75 µl of blocking buffer consisting of 1% w/v of BSA in a TBS buffer (15 mM Trizma-acetate, 136 mM NaCl & 2 mM KCl). Afterwards, plates were washed three times using the washing buffer. As controls, Mouse IgG1 Isotype Control UNLB (Imtec Diagnostics, Ardmore, OK, United States; catalog no 0102-01) was used to generate a two-fold serial dilution from 1/500 to 1/512000 and Mouse IgE Isotype Control (UNLB), Southern Biotech (Imtec Diagnostics, Ardmore, OK, United States; catalog no 0114-01) was used to generate a two-fold serial dilution from 1/1000 to 1/1024000. Serum samples were two-fold diluted from 1/40 to 1/1280. The dilution buffer consisted of 0.1% w/v Tween-20 and 1% BSA in the aforementioned TBS buffer. Plates were loaded with 20 µl/well of the standards and diluted samples and incubated for 90 minutes at room temperature. Another three wash steps were performed before loading 20 µl/well of a 1/500 dilution of the 2nd antibody, Goat anti-mouse IgG1-AP, Southern Biotech (Imtec diagnostics, Ardmore, OK, United States; catalog no 1071-04) or Goat anti-mouse IgE-AP, Southern Biotech (Imtec diagnostics, Ardmore, OK, United States; catalog no 1110-04), respectively. The final three wash steps were performed before loading 40 µl/well of the substrate solution, which consists of 0.5 mg/ml phosphate substrate Sigma-Aldrich, St. Louis, MO, United States; catalog no. S0642-200 TAB) in a 1 mM AMP and 0.1 mM $MgCl_2 \cdot 6H_2O$. Plates were incubated for 1 hour at 37°C before they were read at 405 nm using a SpectraMax ABS PLUS spectrophotometer (Molecular Devices, San Jose, CA, United States).

RT-qPCR

Targeted analysis of cytokine and transcription factor expression was determined by RT-qPCR of RNA extracted from mesenteric lymph nodes (MLN) and colonic tissue (colon). The cDNA library was prepared by combining 500 µM dNTP Set (100 mM) Solution (Invitrogen, Waltham, USA), 2.5 µM Random Primers (Invitrogen), 100 ng/µl of RNA sample and 1ul of ddH2O per sample, followed by heating to 65°C for 5 min and incubation on ice for at least 1 min. Next, 1× SSIV Buffer, 100 mM DTT, 40 U RNaseOUT (Invitrogen, Waltham, USA), Recombinant Ribonuclease Inhibitor (Invitrogen, Waltham, USA), and 200 U Superscript IV Reverse Transcriptase (Invitrogen, Waltham, USA) was added to each sample and incubated at 23°C for 10 min. Samples were incubated at 50°C for 10 min, then heat-inactivated at 80°C for 10 min. A master mix consisting of 1× Buffer, 2.5 mM $MgCl_2$, 400uM dNTP, 1× SYBR Green I Nucleic Acid Gel Stain, 10,000× concentrate in DMSO

(Invitrogen, Waltham, USA), and 0.5 U Platinum *Taq* DNA Polymerase (Life Technologies, Carlsbad, USA), was added to 1 µl each cDNA sample along with 0.2 µM each of forward and reverse primers (the specific primers are listed in **Table S4)**. The PCR cycle consisted of pre-denaturation at 94°C for 5 min, followed by 40 cycles of 20 sec denaturation at 94°C, 50 sec annealing at 60°C, and 45 sec extension at 72°C. Samples were held at 72°C for 5 min post-extension and then a melting curve was generated by heating from 65°C to 95°C with 0.3°C interval increases over 15 sec.

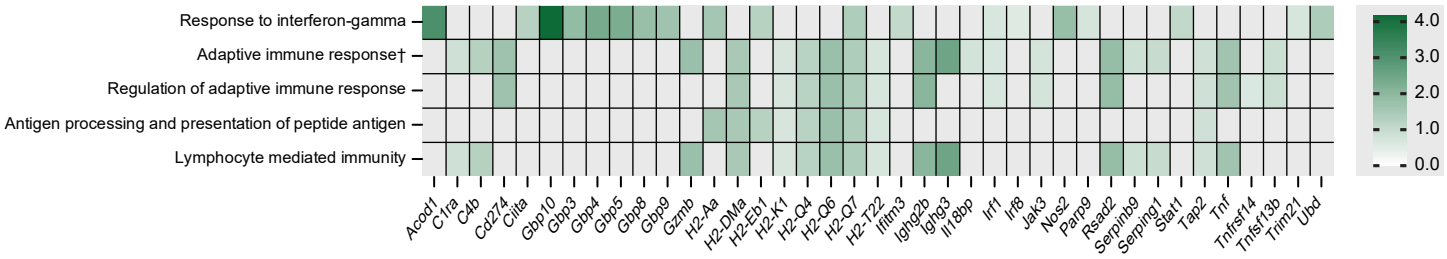
Response to interferon-gamma
Adaptive immune response†
Regulation of adaptive immune response
Antigen processing and presentation of peptide antigen
Lymphocyte mediated immunity
Acod1
C1ra
C4b
Cd274
Ciita
Gbp10
Gbp3
Gbp4
Gbp5
Gbp8
Gbp9
Gzmb
H2-Aa
H2-DMa
H2-Eb1
H2-K1
H2-Q4
H2-Q6
H2-Q7
H2-T22
Ifitm3
Ighg2b
Ifng3
Il18bp
Irf1
Irf8
Jak3
Nos2
Parp9
Rsad2
Serpinb9
Serping1
Stat1
Tap2
Tnf
Tnfrsf14
Tnfsf13b
Trim21
Ubd
4.0
3.0
2.0
1.0
0.0

Figure S1

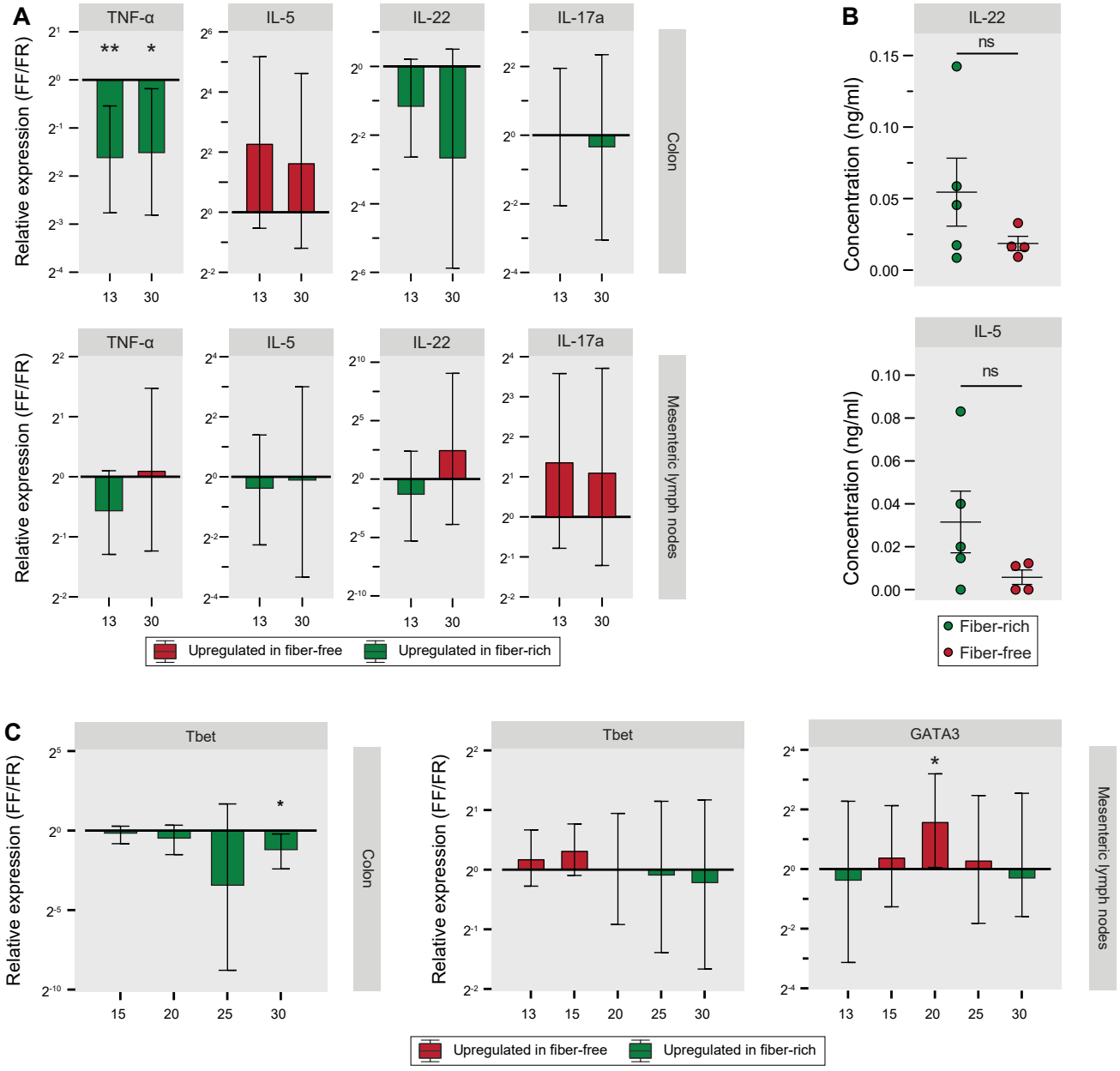
A
TNF-α
IL-5
IL-22
IL-17a
Relative expression (FF/FR)
Colon
Mesenteric lymph nodes
Upregulated in fiber-free
Upregulated in fiber-rich
B
IL-22
IL-5
ns
Concentration (ng/ml)
Fiber-rich
Fiber-free
C
Tbet
GATA3
Relative expression (FF/FR)
Colon
Mesenteric lymph nodes
Upregulated in fiber-free
Upregulated in fiber-rich

Figure S2

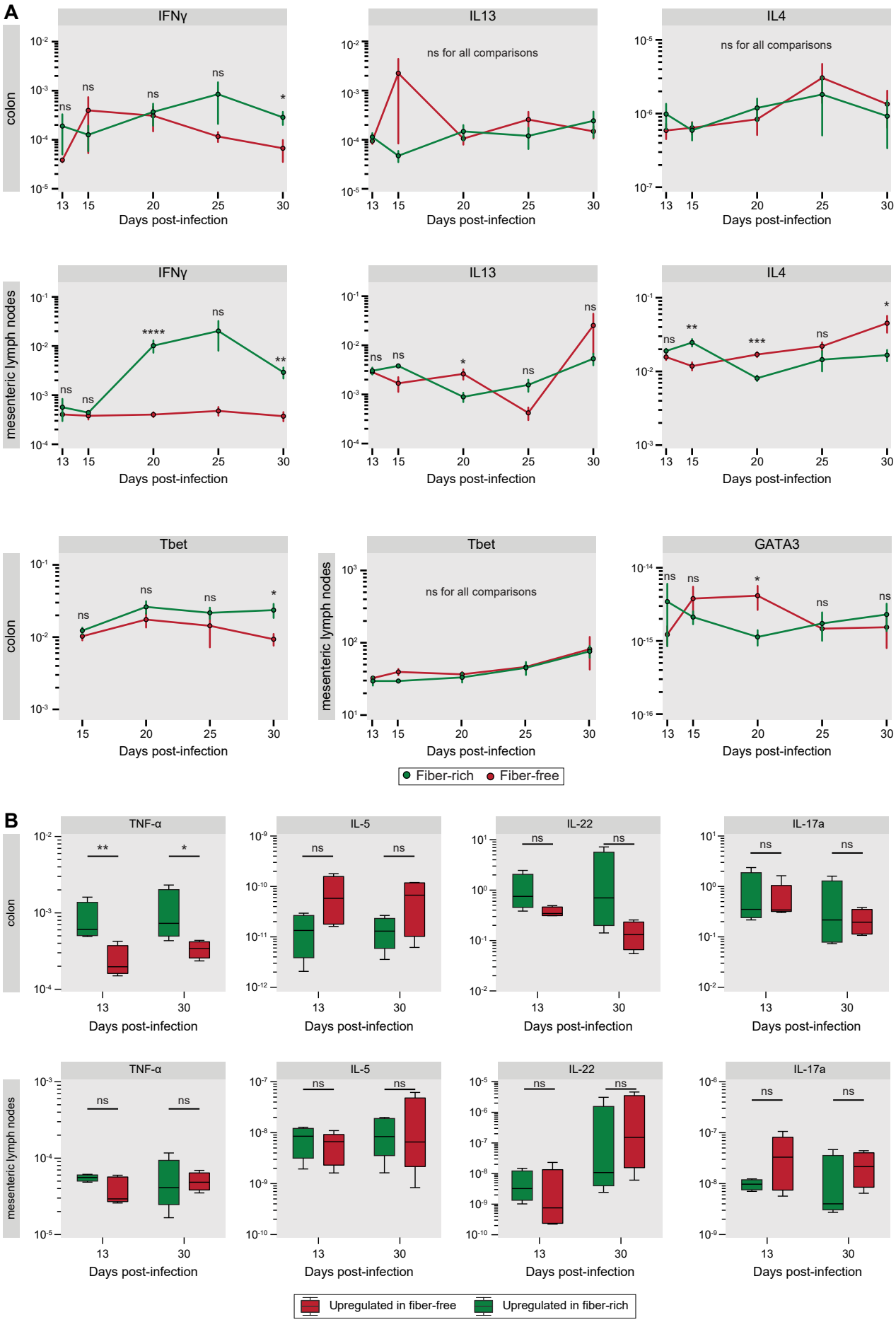
A
IFNγ
IL13
IL4
colon
mesenteric lymph nodes
ns for all comparisons
Days post-infection
Tbet
GATA3
Fiber-rich
Fiber-free
B
TNF-α
IL-5
IL-22
IL-17a
Upregulated in fiber-free
Upregulated in fiber-rich

Figure S3